nature communications

Article

https://doi.org/10.1038/s41467-025-60540-8

Viscoelastic N-cadherin-like interactions maintain neural progenitor cell stemness within 3D matrices

Received: 8 November 2024

Accepted: 28 May 2025

Published online: 05 June 2025

Check for updates

Michelle S. Huang[1,2], Bauer L. LeSavage[3], Sadegh Ghorbani[4,5], Aidan E. Gilchrist[6], Julien G. Roth[7,8], Carla Huerta-López[4], Esther A. Mozipo[3], Renato S. Navarro[4] & Sarah C. Heilshorn[4]

Neural progenitor cells (NPCs) hold immense potential as therapeutic candidates for neural regeneration, and materials-based strategies have emerged as attractive options for NPC expansion. However, maintaining NPC stemness has proven challenging in vitro, due to their propensity to form cell-dense neurospheres. While neurospheres promote cell–cell interactions required for NPC stem maintenance, they also restrict oxygen transport, leading to hypoxia and limited cell expansion. To overcome these limitations, we investigate two materials-based approaches to maintain NPC stemness: 1) physical matrix remodeling within a viscoelastic, stress-relaxing hydrogel and 2) matrix-induced N-cadherin-like signaling through a cell-instructive peptide. While viscoelasticity alone is sufficient to maintain NPC stemness compared to an elastic environment, NPCs still preferentially form neurospheres. The addition of N-cadherin-like peptides promotes a distributed culture of NPCs while maintaining their stemness through cadherin-mediated signaling, ultimately exhibiting improved long-term expansion and neural differentiation. Thus, our findings reveal matrix viscoelasticity and engineered N-cadherin-like interactions as having a synergistic effect on NPC expansion and differentiation within 3D matrices.

Neural progenitor cells (NPCs) are a promising source for nervous system regenerative therapies, as they can differentiate into neurons, astrocytes, and oligodendrocytes[1–3]. However, a critical limitation preventing clinical translation is the inability to efficiently and reproducibly expand NPCs in vitro while maintaining their stem cell phenotype[4]. Loss of NPC stemness is also observed in vivo throughout the aging process and in pathological disease states, causing diminished ability for NPC self-renewal and biased differentiation[5–7]. These phenotypic abnormalities are due in part to complex environmental changes in the stem cell niche, including altered extracellular matrix (ECM) biochemical and biomechanical properties[8–10]. Therefore, understanding the role of cell–cell and cell–matrix interactions in the NPC niche is critical to revealing the required signals that enable NPC stemness maintenance to achieve efficient cell expansion while retaining their differentiation capacity.

[1]Department of Chemical Engineering, Stanford University, Stanford, CA, USA. [2]The Institute for Chemistry, Engineering & Medicine for Human Health (Sarafan ChEM-H), Stanford University, Stanford, CA, USA. [3]Department of Bioengineering, Stanford University, Stanford, CA, USA. [4]Department of Materials Science and Engineering, Stanford University, Stanford, CA, USA. [5]Department of Health Technology, Technical University of Denmark, Lyngby, Denmark. [6]Department of Biomedical Engineering, University of California, Davis, Davis, CA, USA. [7]Institute for Stem Cell Biology and Regenerative Medicine, Stanford University School of Medicine, Stanford, CA, USA. [8]Complex In Vitro Systems, Safety Assessment, Genentech Inc., South San Francisco, CA, USA. e-mail: heilshorn@stanford.edu

Traditionally, NPCs are cultured in two-dimensional (2D) monolayers or as three-dimensional (3D) neurospheres because they are highly density dependent. Neurosphere culture allows cells to be maintained as large 3D cell clusters, resulting in a significant increase in the total number of cells per surface area compared to 2D planar culture[11,12]. NPCs are able to survive, self-renew, and differentiate throughout neurosphere culture. Unfortunately, neurosphere culture remains limited in overall cell expansion due to size limitations that inhibit oxygen diffusion into the cell-dense core, causing necrosis[13,14]. In both 2D monolayers and 3D neurospheres, the cells are present in non-representative geometries that preclude the formation of distributed 3D cellular networks. To overcome these challenges, the use of 3D synthetic matrices has emerged as an alternative approach to influence stem cell behavior for cell expansion and manufacturing. Unlike surface area-limited 2D cultures or diffusion-limited neurosphere cultures, synthetic matrices can provide 3D instructive cues to support scalable cell expansion for potential cell-based therapies[15–17]. Thus, the development of 3D biomaterials to support the long-term expansion of NPCs that results in a stem-like homogeneous, distributed, and network-forming population would greatly increase their potential therapeutic relevance.

Biochemical and biophysical factors of the microenvironment play a key role in directing stem cell behavior within the native stem cell niche[18–20]. Previous studies have identified cell-adhesive ligand composition[21,22], matrix stiffness[23,24], and stress relaxation rate[25,26] as important parameters for modulating NPC differentiation and fate acquisition. In contrast to these previous studies, we are interested in identifying the signaling cues that will support the high-density culture of viable NPCs in an undifferentiated, stem-like state that still maintain the capacity to differentiate. In embedded 3D cultures of NPCs, we have previously shown that matrix remodelability impacts stemness maintenance, with gels that are more remodelable significantly improving NPC differentiation capacity[17,27]. Specifically, we found that proteolytic matrix degradation allows encapsulated NPCs to spread within the material to form N-cadherin-mediated cell–cell contacts, leading to downstream stem cell maintenance. These cell–cell contacts and N-cadherin engagement subsequently activate β-catenin signaling, which plays a significant role in the regulation of the stem cell phenotype. Thus, it is not matrix degradation per se that enables robust stemness maintenance, but rather the presence of cell–cell interactions. Cells can remodel their matrix in several ways, including permanent enzymatic remodeling of degradable matrices and dynamic network remodeling of viscoelastic and viscoplastic matrices[28]. As matrix stress relaxation enables degradation-independent, cell-directed matrix remodeling, we hypothesized that a viscoelastic, stress-relaxing matrix would promote NPC proliferation and stemness maintenance through increasing cell–cell contact.

Viscoelastic materials, such as brain tissue, undergo remodeling in response to cell-imposed forces[29]. In comparison to purely elastic materials, viscoelastic hydrogels that exhibit stress relaxation promote cell spreading, migration, and proliferation in 3D[25,30,31], which we reasoned would lead to cell–cell interactions important for maintaining NPC stemness. Stress relaxation can be engineered within hydrogels through various strategies, including polymer entanglements, weak physical associations, and dynamic covalent chemistry[29]. Here, we leveraged dynamic covalent hydrazone bonds to introduce stress relaxation into hyaluronic acid (HA) and elastin-like protein (ELP) engineered hydrogels. We have previously demonstrated that varying the ratio of benzaldehyde-functionalized HA and aldehyde-functionalized HA can afford precise control over the crosslinking kinetics, and therefore, the stress relaxation rate, of the resulting hydrogels[25].

HA was chosen due to its high prevalence in the native brain ECM[32], while the engineered ELP was selected for its modular tunability to directly specify the concentration of different cell-adhesive peptide motifs[33–35]. Specifically, we use ELP variants containing a fibronectin-derived, integrin-engaging RGD peptide that is known to support the culture of NPCs and differentiated neural cell types[36–38]. Additionally, to directly engage the N-cadherin receptors responsible for cell–cell signaling in NPCs, we engineered a new ELP variant containing an N-cadherin-derived HAVDI peptide. Early sequencing and inhibition studies initially identified the HAVDI motif from the first extracellular domain (EC1) of N-cadherin as a cadherin cell adhesion site[39–41]. While the HAVDI peptide alone cannot mimic all aspects of N-cadherin function[42], several studies have demonstrated its antagonistic activity as a soluble peptide in modulating fibroblast adhesion and neurite outgrowth in vitro[41,43]. By instead tethering the HAVDI peptide to matrices, it was able to act as an N-cadherin agonist in several applications, including influencing the morphology and fate commitment of mesenchymal stromal cells[44–47], promoting neurogenesis of neural stem cells[48], directing cell fate and diversity in neural organoids[49], and supporting the formation of synaptically connected neurons[50]. As cell–cell contact plays an important role in maintaining NPC stemness, we hypothesized that incorporation of HAVDI within our designer, viscoelastic matrix would promote NPC stemness maintenance and enhance differentiation capacity.

Here, we develop a modular, 3D engineered hydrogel platform to define the necessary matrix properties for robust NPC expansion and differentiation in vitro. We demonstrate that in the absence of HAVDI, matrix viscoelasticity is required for NPC proliferation in the form of neurospheres, where cell–cell contact between cells within the neurospheres is sufficient to maintain stemness. When RGD and HAVDI peptides are simultaneously incorporated into fast-relaxing, viscoelastic hydrogels, NPCs no longer form neurospheres and instead form a distributed 3D network of NPCs throughout the hydrogel. Distributed 3D NPC cultures are able to undergo long-term expansion, exhibit high viability, and maintain the capacity to differentiate into glial cells and neurotransmitter-responsive neurons. Ultimately, our results suggest that the combination of matrix viscoelasticity and engineered N-cadherin-like interactions can regulate the phenotype of encapsulated NPCs to maintain their stem cell phenotype and differentiation capacity in vitro.

Results

Matrix stress relaxation enables cell–cell contact-mediated stemness maintenance

To first assess the role of matrix remodelability, we evaluated NPC stemness maintenance in a family of materials with differing stress relaxation rates and identical biopolymer compositions. We recently developed a family of engineered viscoelastic matrices consisting of HA and ELP, which we term HELP. HELP hydrogels have independently tunable stress relaxation rates, stiffness, and cell-instructive ligand density[25,51]. Here, the HA (1 wt%) and ELP (1 wt%) polymers were crosslinked using either static or dynamic covalent bonds (Fig. 1a, b). Stress-relaxing HELP gels were formed by modifying HA with either an aliphatic aldehyde (fast exchange kinetics) or benzaldehyde (slow exchange kinetics) functional group. When combined with hydrazine-modified ELP, dynamic covalent hydrazone bonds form, resulting in a viscoelastic, stress-relaxing hydrogel (Fig. 1a). Elastic, non-stress-relaxing HELP gels were formed by combining a tetrazine-modified HA with a norbornene-modified ELP to form static covalent crosslinks (Fig. 1b). All hydrogels were formed with a shear elastic modulus of ~800 Pa (Fig. 1c, Supplementary Fig. 1a, b), which falls within the range of stiffness reported for native brain tissue and has been demonstrated to support both neuronal and glial differentiation[27,52,53]. Additionally, these hydrogels all included 1 mM of an extended cell-adhesive arginylglycylaspartic acid (RGD) peptide derived from fibronectin in the ELP polymer backbone. RGD is known to engage several cell surface receptors, including integrin subunit β1, which has been shown to

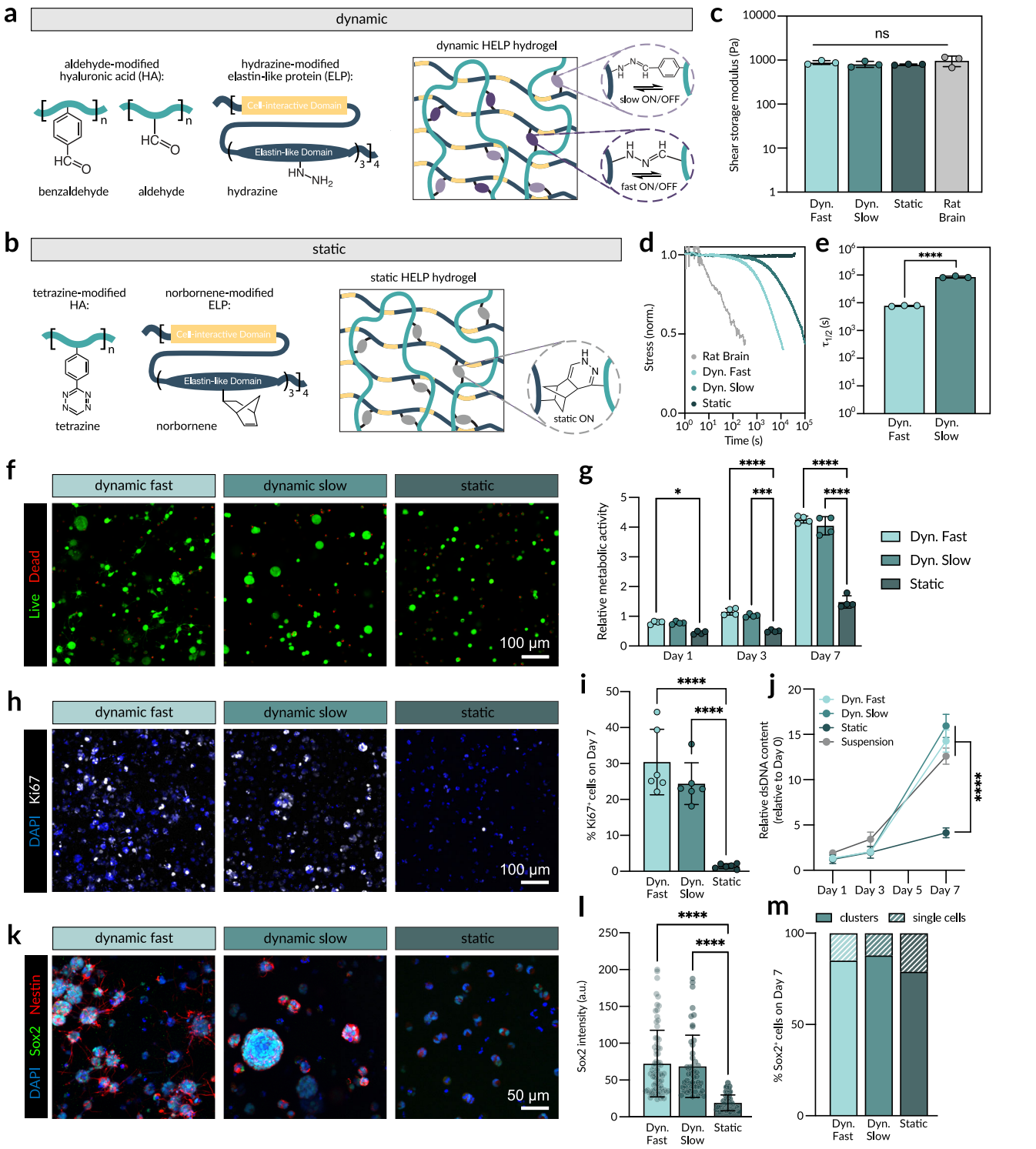

regulate NPC function in vivo and support cell adhesion and neurite outgrowth in vitro[36,54–56].

To control the stress relaxation rate of the viscoelastic HELP gels, we varied the ratio of aldehyde- to benzaldehyde-functionalized HA to be 0:100 or 50:50, resulting in Dynamic Slow and Dynamic Fast HELP gels, respectively. Shear rheology confirmed that the stress relaxation rate of the dynamic HELP hydrogels could be tuned independently of matrix stiffness (Fig. 1d). The stress relaxation half-life ($\tau_{1/2}$), which is defined as the time required for the stress to reach half its initial value under a constant applied strain, ranged from ~10^4 s for Dynamic Fast gels to ~10^5 s for Dynamic Slow gels (Fig. 1e). As expected, Static gels did not relax in response to the applied strain even after 24 h. While the stress relaxation rates of the dynamic HELP hydrogels are slower than those of native rat brain tissue (Fig. 1d), this family of HELP gels presents a tunable system for reproducibly controlling matrix stress relaxation over timescales known to impact NPCs[25]. All three crosslinking chemistries were highly cytocompatible, as NPCs dissociated into single cell suspensions could be encapsulated within the HELP gels with high viability (>90%) (Fig. 1f, Supplementary Fig. 2a).

We next investigated the capability of NPCs to maintain stemness within hydrogels of different stress relaxation rates. As progenitor cells, a hallmark of NPC stemness maintenance is the ability to self-

Fig. 1 | 3D matrix stress relaxation is required for NPC stemness maintenance. **a** Schematic of Dynamic HELP gels (Dynamic Fast or Dynamic Slow), which are composed of aldehyde- or benzaldehyde-modified hyaluronic acid (HA) and hydrazine-modified elastin-like protein (ELP) crosslinked through dynamic covalent bonds. **b** Schematic of Static HELP gels, which are composed of tetrazine-modified HA and norbornene-modified ELP crosslinked through static covalent bonds. **c** Shear storage moduli of rat brain and all three HELP gel formulations ($N = 3$ independent runs, data are means ± standard deviation). **d** Normalized representative stress relaxation profiles for rat brain and all three HELP gel formulations. **e** Stress relaxation half-lives ($\tau_{1/2}$) of Dynamic Fast and Dynamic Slow HELP gels ($N = 3$ independent runs, data are means ± standard deviation). ****$p < 0.0001$. **f** Representative maximum projection fluorescence images of NPCs encapsulated within all three HELP gel formulations after 7 days of culture with calcein AM labeled live cells (green) and ethidium homodimer-1 labeled dead cells (red). **g** Quantification of the relative metabolic activity of encapsulated NPCs over time, relative to the activity 1 hour post-encapsulation ($N = 4$ replicate hydrogels, data are means ± standard deviation). Day 1: Dynamic Fast vs. Static *$p = 0.0397$; Day 3: Dynamic Slow vs. Static ***$p = 0.0004$, Dynamic Fast vs. Static ****$p < 0.0001$; Day 7: Dynamic Fast vs. Static, Dynamic Slow vs. Static ****$p < 0.0001$. **h** Representative maximum projection fluorescence images of NPCs encapsulated within all three HELP gel formulations after 7 days of culture with labeled cells in active phases of the cell cycle (Ki67, white). Nuclei are counterstained with DAPI (blue). **i** Quantification of the percentage of Ki67+ cells after 7 days in culture ($n = 6$ randomized field of views, $N = 3$ replicate hydrogels, data are means ± standard deviation). ****$p < 0.0001$. **j** Quantification of the relative dsDNA content of encapsulated NPCs over time ($N = 4$ replicate hydrogels, data are means ± standard deviation) compared to suspension neurosphere cultures. ****$p < 0.0001$. **k** Representative maximum projection fluorescence images of NPCs encapsulated within all three HELP gel formulations after 7 days of culture labeled with the neural stem cell markers Nestin (red) and Sox2 (green). Nuclei are counterstained with DAPI (blue). **l** Quantification of Sox2 intensity after 7 days in culture ($n = 75$ single cells for Dynamic Fast, 50 single cells for Dynamic Slow, and 57 single cells for Static, data are means ± standard deviation). a.u., arbitrary units. ****$p < 0.0001$. **m** Quantification of the percentage of Sox2+ cells that are in clusters vs. single cells after 7 days in culture ($N = 5$ replicate hydrogels). Statistical analyses performed as one-way ANOVA with Tukey's multiple comparisons test (**c**, **i**, **m**), two-tailed unpaired t test (**e**), two-way ANOVA with Tukey's multiple comparisons test (**g**, **j**), and Kruskal-Wallis with Dunn's multiple comparisons test (**l**). Source data are provided as a Source Data file.

renew. Over 7 days in maintenance medium, NPCs exhibited significantly higher rates of metabolic activity in Dynamic Fast and Dynamic Slow gels, compared to Static gels (Fig. 1g), suggesting that cells may be more proliferative in stress-relaxing matrices. Immunostaining for the proliferation marker Ki67 further revealed that NPCs within both dynamic gels maintained significantly higher percentages of cells in an active proliferative state (~30% and ~24% in Dynamic Fast and Dynamic Slow, respectively, compared to ~1.4% in Static) (Fig. 1h, i). Similarly, a significantly higher total number of cells was present within Dynamic Fast and Dynamic Slow gels at day 7 compared to Static gels (Fig. 1j). Collectively, these data demonstrate that while all hydrogel conditions supported NPC viability, the static, non-stress-relaxing condition led to decreased proliferation, resulting in limited potential for expansion.

Changes in NPC stemness were further evaluated by performing immunostaining and immunoblotting for the classical NPC stemness markers, Nestin and Sox2[12,57]. NPCs encapsulated within Dynamic Fast and Dynamic Slow gels expressed Nestin and Sox2 at significantly higher levels than those encapsulated within Static gels (Fig. 1k, Supplementary Fig. 2b, c). Furthermore, a higher percentage of Sox2+ cells was observed in Dynamic Fast (~82%) and Dynamic Slow (~76%) gels compared to Static (~25%) gels (Supplementary Fig. 2d). At an individual cell level, the Sox2 intensity per cell was also higher in Dynamic Fast and Dynamic Slow gels compared to Static gels (58.3 and 54.5 vs 15.0 a.u., respectively, Fig. 1l). No significant differences in proliferation or Nestin and Sox2 expression were observed as a function of stress relaxation rate for the two dynamic gels. These data suggest that NPCs are able to maintain stemness within stress-relaxing hydrogels, whereas they exhibit a loss of stemness within non-stress-relaxing, elastic hydrogels.

Since NPCs rely on cell–cell contact to maintain stemness, we hypothesized that the dynamic HELP gels promoted NPC neurosphere formation, which would then result in cell–cell signaling through adjacent NPCs. Indeed, by day 7, NPCs within both dynamic gels formed multicellular neurospheres, with ~78% and ~75% of cells in Dynamic Fast and Dynamic Slow gels, respectively, found in clusters (Figs. 1k, 2e). In contrast, a majority of NPCs within Static gels (~61%) remained as single cells (Supplementary Fig. 2e). Further, the few neurospheres that formed within Static gels were much smaller in size compared to the neurospheres formed within the dynamic conditions (Supplementary Fig. 2f), and they exhibited decreased proliferation compared to neurospheres in both dynamic hydrogel conditions and suspension culture (Fig. 1j), suggesting that matrix confinement may inhibit NPC expansion. Interestingly, most of the Sox2+ cells within all hydrogel conditions were found within neurospheres (~85% in Dynamic Fast, ~88% in Dynamic Slow, ~79% in Static), regardless of neurosphere size (Fig. 1m), with a greater number of Sox2+ cells per neurosphere as the neurosphere diameter increased (Supplementary Fig. 2g). Even in the Static gels, where significantly fewer neurospheres formed, NPCs within clusters expressed Sox2 (Supplementary Fig. 2h). Across all hydrogel conditions, the single cells lost expression of Nestin and Sox2 (Supplementary Fig. 2h). Because the majority of NPCs within Static gels were single cells, this non-stress-relaxing condition was insufficient at maintaining NPC stemness. Taken together, these results indicate that NPC stemness relies on cell–cell interactions, which are favored by matrix remodelability, when encapsulated within 3D matrices.

N-cadherin adhesive interactions enable stemness maintenance of a distributed 3D NPC culture

While dynamic HELP hydrogels were able to maintain NPC stemness over 7 days, the NPCs within these hydrogels were expanding as neurospheres. Neurosphere culture has several limitations, including: (1) heterogeneous cell populations, (2) limited ability to control spontaneous NPC differentiation, and (3) necrotic cores due to poor oxygen and nutrient transport through the cell-dense spheres[13,14]. Neurosphere formation is also not representative of the physiological organization of NPCs in vivo[58]. During neural development, NPCs do not exist as neurospheres, but instead extend processes outwards from the cell body towards the ventricular and pial surfaces, which later serve as guides along which differentiating neurons migrate[59]. Within this developing niche, N-cadherin is broadly expressed and contributes to the strong adhesion between NPCs to maintain tissue architecture[60]. We therefore hypothesized that a 3D matrix that is both remodelable and mimics the broad expression of N-cadherin present in the developing brain would allow for dispersed NPC cultures that maintain NPC stemness without forming neurospheres.

To explore the possibility that N-cadherin adhesive interactions may regulate NPC morphology and stemness maintenance in 3D cultures, we engineered our dynamic HELP gels to present both integrin-binding and N-cadherin peptide motifs, modeling both cell–ECM and cell–cell interactions, respectively (Fig. 2a). The modular ELP component of HELP hydrogels can be designed to present a variety of cell-instructive ligands through specification of the primary amino acid sequence. Our group has previously cloned and reported on a library of ELPs with tunable ligands derived from several ECM proteins[33]. Here, we expand on this library by engineering a new ELP containing an N-cadherin-derived HAVDI sequence in the protein backbone

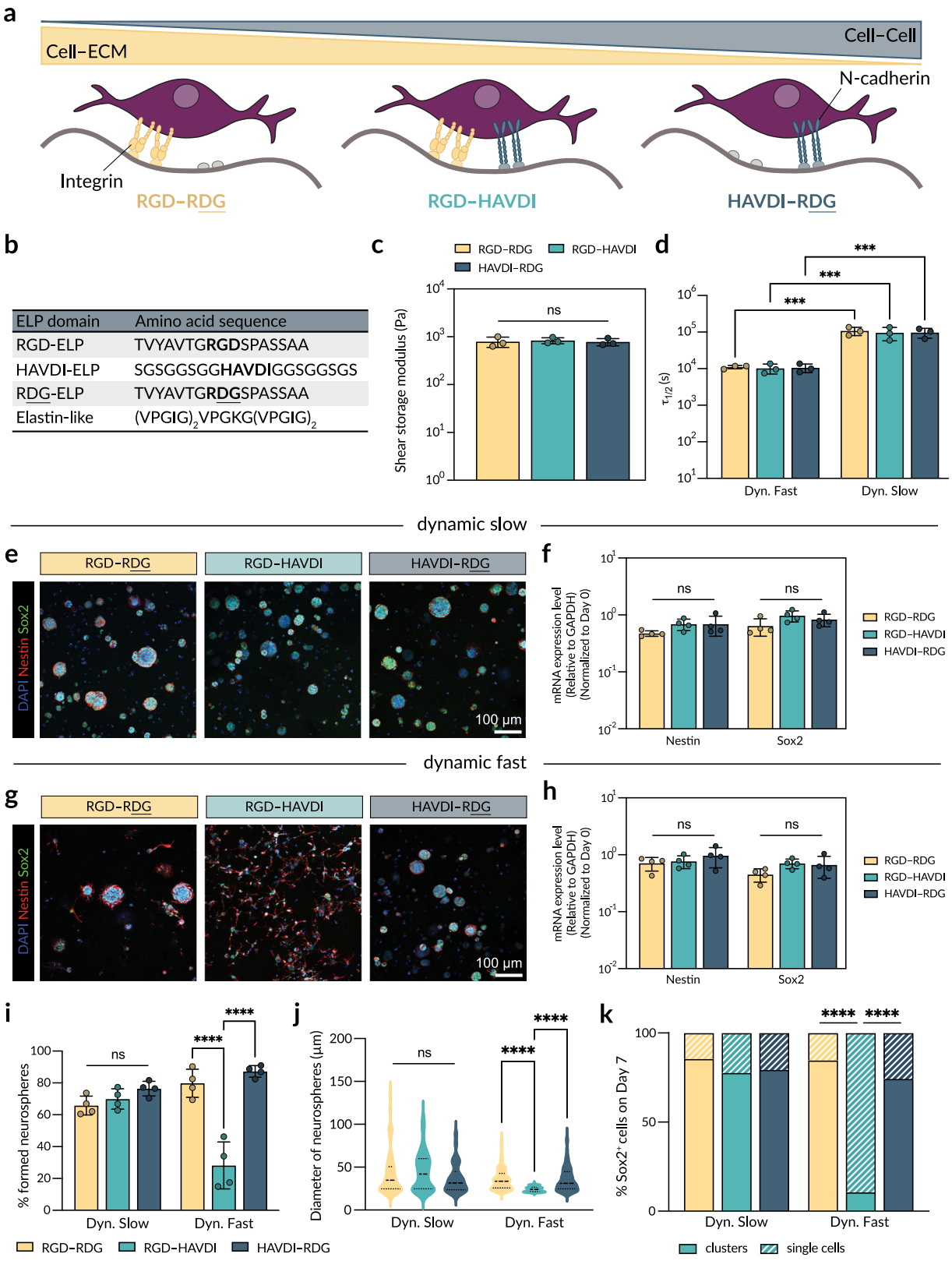

ELP domain	Amino acid sequence
RGD-ELP	TVYAVTG**RGD**SPASSAA
HAVDI-ELP	SGSGGSGG**HAVDI**GGSGGSGS
RDG-ELP	TVYAVTG**RDG**SPASSAA
Elastin-like	$(VPGIG)_2VPGKG(VPGIG)_2$

(Supplementary Fig. 3). To enhance conformational flexibility, a flexible GGS repeat is incorporated flanking the HAVDI sequence. Engineered ELPs with the following sequences were successfully cloned and expressed: (1) an N-cadherin-derived HAVDI sequence to artificially induce cell–cell signaling, (2) a fibronectin-derived, integrin-binding RGD sequence to mimic cell–matrix signaling, and (3) a scrambled, cell-inert RDG sequence to which cells cannot bind (Fig. 2b). The biochemical identity of these three ELPs was confirmed through amino acid analysis, demonstrating excellent agreement between the theoretical and observed amino acid frequencies for the designed ELP sequences (Supplementary Fig. 4).

Several in vitro studies have demonstrated that the co-presentation of both RGD and HAVDI peptides at equimolar concentrations improves cell adhesion over HAVDI alone for

Fig. 2 | HAVDI/RGD co-presentation within fast stress-relaxing matrices permits NPC stemness maintenance as a distributed 3D culture. a Schematic representation of the engineered peptides (RGD, HAVDI, RDG negative control) used in this study to emulate both cell–ECM and cell–cell interactions through integrin and N-cadherin receptors, respectively. **b** Amino acid sequences for the bioactive domains of RGD-, HAVDI-, and negative control RDG-ELP variants, as well as the elastin-like sequence used for all ELPs. **c** Shear storage moduli of Dynamic Slow HELP gel formulations with different ligand combinations ($N = 3$ independent runs, data are means ± standard deviation). **d** Stress relaxation half-lives ($\tau_{1/2}$) of Dynamic Fast and Dynamic Slow HELP gels with different ligand combinations ($N = 3$ independent runs, data are means ± standard deviation). RGD-RDG: $^{***}p = 0.0002$; RGD-HAVDI: $^{***}p = 0.0006$; HAVDI-RDG: $^{***}p = 0.0005$. NPCs encapsulated within either Dynamic Slow (**e**, **f**) or Dynamic Fast (**g**, **h**) HELP gels after 7 days of culture were immunolabeled for Nestin (red) and Sox2 (green) with nuclei counterstained (blue) (**e**, **g**) and analyzed for mRNA expression of *Nestin* and *Sox2* (**f**, **h**) ($N = 4$ replicate hydrogels, data are means ± standard deviation). **i** Quantification of the percentage of neurospheres formed after 7 days in culture ($N = 4$ replicate hydrogels, data are means ± standard deviation). $^{****}p < 0.0001$. **j** Quantification of the diameter of neurospheres after 7 days in culture ($n = 175$ neurospheres for Dynamic Slow RGD-RDG, 99 neurospheres for Dynamic Slow RGD-HAVDI, 127 neurospheres for Dynamic Slow HAVDI-RDG, 47 neurospheres for Dynamic Fast RGD-RDG, 54 neurospheres for Dynamic Fast RGD-HAVDI, and 31 neurospheres for Dynamic Fast HAVDI-RDG, medians and quartiles denoted by dotted lines). $^{****}p < 0.0001$. **k** Quantification of the percentage of Sox2+ cells that are in clusters vs. single cells after 7 days in culture ($N = 4$ replicate hydrogels). $^{****}p < 0.0001$. Statistical analyses performed as one-way ANOVA with Tukey's multiple comparisons test (**c**), two-way ANOVA with Tukey's multiple comparisons test (**d**, **f**, **h**, **i**, **k**), and Kruskal-Wallis with Dunn's multiple comparisons test (**j**). Source data are provided as a Source Data file.

mesenchymal stromal cells and neural stem cells[46,48]. Additionally, integrin–cadherin crosstalk can alter the mechanosensing of viscoelasticity in 2D[61]. Therefore, we blended our ELP variants at 1:1 ratios of RGD:HAVDI, RGD:RDG, and HAVDI:RDG before combining them with our modified HA to create HELP gels that present both ligands, RGD only, and HAVDI only, respectively. This experimental design allowed us to maintain constant biopolymer concentrations (1 wt% ELP and 1 wt % HA) across all hydrogels. Shear rheology confirmed that all six dynamic hydrogels exhibited similar gelation profiles and hydrogel stiffness (Fig. 2c, Supplementary Fig. 5). Finally, blending of the different ELP variants resulted in similar stress relaxation rates for both the family of Dynamic Slow HELP gels and the family of Dynamic Fast HELP gels (Fig. 2d).

Single cell suspensions of NPCs were encapsulated within the Dynamic Slow and Dynamic Fast HELP gels displaying different ligand combinations (RGD-RDG, RGD-HAVDI, and HAVDI-RDG) (Fig. 2a). After 7 days of culture, NPCs remained highly viable (> 90%) in all hydrogel conditions (Supplementary Fig. 6a, b). In Dynamic Slow HELP gels, the NPCs formed neurospheres regardless of ligand presentation (Fig. 2e, Supplementary Fig. 6c). Accordingly, the NPCs were able to maintain expression of stemness markers, Nestin and Sox2, due to cell–cell contact provided by adjacent cells within the neurosphere. mRNA expression of *Nestin* and *Sox2* was also statistically similar across all Dynamic Slow conditions (Fig. 2f). In Dynamic Fast HELP gels, striking differences in NPC morphology emerged as a function of ligand presentation. Similar to the Dynamic Slow conditions, NPCs in RGD-RDG and HAVDI-RDG matrices also formed neurospheres (Fig. 2g, Supplementary Fig. 6c). However, NPCs in Dynamic Fast RGD-HAVDI matrices exhibited a spread, elongated morphology and extended Nestin+ projections throughout the hydrogel while remaining primarily singularized (Fig. 2g, Supplementary Fig. 6c). These morphological differences only emerged in Dynamic Fast gels that presented both RGD and HAVDI ligands.

Although NPCs within Dynamic Fast RGD-HAVDI gels often remained distributed as single cells with minimal cell–cell contact, they still maintained expression of *Nestin* and *Sox2* (Fig. 2h). Western blot analysis confirmed that Nestin and Sox2 expression were also maintained at the protein-level (Supplementary Fig. 6d, e). NPCs within Dynamic Fast RGD-HAVDI gels formed significantly fewer neurospheres (~28%) compared to NPCs within the other hydrogel conditions (~76% average), which were all statistically similar (Fig. 2i). The neurospheres that formed within the Dynamic Fast RGD-HAVDI gels were also much smaller than those in the other Dynamic Fast and all Dynamic Slow hydrogel conditions (Fig. 2j). In the Dynamic Fast RGD-HAVDI gels, ~89% of Sox2+ cells were found as single cells rather than cells in clusters (Fig. 2k). In comparison, in the other hydrogel formulations, most of the Sox2+ cells (~80% average) were found in clusters (Fig. 2k). Despite these differences in morphology, NPCs in all Dynamic Fast hydrogel conditions were able to proliferate. Consistent with previous reports, hydrogels that included the RGD ligand (either with or without the HAVDI ligand) had slightly increased proliferation by day 7 (Supplementary Fig. 6f).

Taken together, these data suggest that co-presentation of RGD and HAVDI ligands within Dynamic Fast HELP gels is sufficient to enable stemness maintenance of a distributed 3D culture of NPCs. Interestingly, co-presentation of these ligands within Dynamic Slow HELP gels still resulted in neurosphere formation, suggesting that the slow relaxation timescale of Dynamic Slow gels may result in cellular confinement. Consistent with this idea, neurospheres within Dynamic Slow gels exhibited smooth neurosphere boundaries with no neuritic projections (Fig. 2e, g), while neurospheres within Dynamic Fast gels (either RGD only or HAVDI only) extended small projections radially outwards (Supplementary Fig. 6c). The neuritic projections from neurospheres within Dynamic Fast gels were similar in length but shorter than the neuritic projections from single cells present in Dynamic Fast RGD-HAVDI gels (Supplementary Fig. 6g). Given that the NPCs within Dynamic Fast RGD-HAVDI gels were able to maintain stemness as single cells, this suggests that N-cadherin signaling may be transmitted through the engineered matrix.

Matrix-induced HAVDI presentation promotes cadherin-mediated β-catenin signaling

We next evaluated whether N-cadherin-like signaling in Dynamic Fast RGD-HAVDI hydrogels was regulated through similar mechanisms as signaling through true N-cadherin cell–cell contacts (i.e., NPCs in neurospheres). N-cadherin is expressed in the adult murine NPCs used here[17], and immunostaining confirmed that NPCs in all hydrogel conditions expressed N-cadherin, suggesting that N-cadherin-mediated contact may be relevant for stemness maintenance in this system (Fig. 3a). Previous work has implicated N-cadherin cell–cell contacts in modulating β-catenin signaling, which has been demonstrated to play a role in maintaining NPC stemness[17,62]. We therefore hypothesized that in the absence of neurosphere formation, HAVDI presentation in this engineered hydrogel was promoting NPC stemness by activating β-catenin signaling through engineered N-cadherin contacts.

To demonstrate that the HAVDI motifs within our engineered hydrogels could stimulate N-cadherin cell-surface receptors, NPCs encapsulated within Dynamic Fast RGD-HAVDI hydrogels were treated with an inhibitor of N-cadherin binding (cyclic HAV peptide)[41]. Within the Dynamic Fast RGD-HAVDI hydrogels, NPCs were mostly present as single cells (Fig. 2g), so the cyclic HAV peptide was expected to primarily block the binding of N-cadherin to HAVDI motifs within the matrix. As expected, preventing N-cadherin binding through this small molecule inhibitor resulted in decreased levels of active (non-phospho S45) β-catenin (Supplementary Fig. 7a, b) and decreased expression of the β-catenin responsive gene *Axin2* (Fig. 3b, c). *MYC* and *CCND1*, other targets of the β-catenin signaling pathway that regulate stem cell self-

https://doi.org/10.1038/s41467-025-60540-8

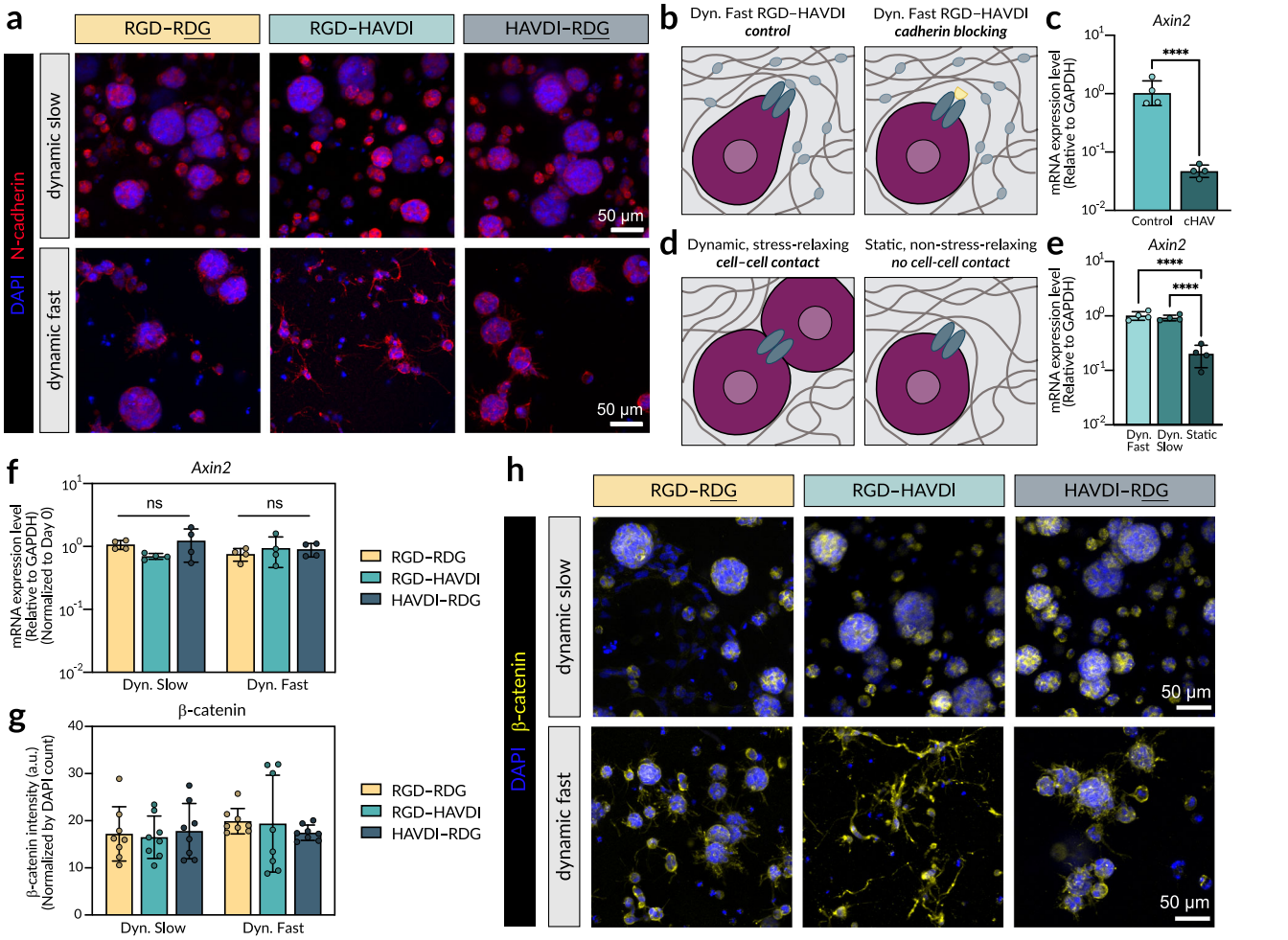

Fig. 3 | HAVDI matrix presentation maintains β-catenin signaling similar to neurospheres. a Representative maximum projection fluorescence images of NPCs encapsulated within Dynamic Slow and Dynamic Fast HELP gels after 7 days of culture labeled with N-cadherin (red) with nuclei counterstained (blue). **b** Schematic of N-cadherin engagement through matrix-presenting HAVDI peptides within Dynamic Fast RGD-HAVDI hydrogels (left) and schematic of N-cadherin blocking with the soluble, cyclic peptide cHAV (right). **c** Gene expression of the β-catenin reporter *Axin2* after 7 days in culture in Dynamic Fast RGD-HAVDI hydrogels with or without the cHAV inhibitor ($N = 4$ replicate hydrogels, data are means ± standard deviation). $^{****}p < 0.0001$. **d** Schematic of a dynamic, stress-relaxing hydrogel that permits cell–cell contact through neurosphere formation (left) and schematic of a static, non-stress-relaxing hydrogel that prevents neurosphere formation (right). **e** Expression of *Axin2* mRNA after 7 days of culture in Dynamic Fast, Dynamic Slow, and Static hydrogels with only the RGD ligand ($N = 4$ replicate hydrogels, data are means ± standard deviation). $^{****}p < 0.0001$. **f** Expression of *Axin2* mRNA after 7 days of culture in Dynamic Slow and Dynamic Fast hydrogels with different ligand combinations ($N = 4$ replicate hydrogels, data are means ± standard deviation). **g** Quantification of β-catenin fluorescence intensity, normalized by cell number, after 7 days in culture in Dynamic Slow and Dynamic Fast hydrogels with different ligand combinations ($n = 8$ randomized field of views, $N = 4$ replicate hydrogels, data are means ± standard deviation). **h** Representative maximum projection fluorescence images of NPCs after 7 days of culture within Dynamic Slow and Dynamic Fast HELP gels labeled with β-catenin (yellow) with nuclei counterstained (blue). Statistical analyses performed as two-tailed unpaired *t* test (**c**), one-way ANOVA with Tukey's multiple comparisons test (**e**), and two-way ANOVA with Tukey's multiple comparisons test (**f**, **g**). Source data are provided as a Source Data file.

renewal[63,64], were also downregulated when cadherin interactions were blocked (Supplementary Fig. 7c, d). Together, these data suggest that β-catenin activity within our viscoelastic engineered hydrogels is specifically due to matrix interactions with N-cadherin receptors. Additionally, NPCs cultured in the presence of the cyclic HAV peptide exhibited decreased expression of Nestin and Sox2 (Supplementary Fig. 7e–h), indicating that the N-cadherin-like signaling within our engineered hydrogels are necessary for maintaining NPC stemness. As a control experiment, we explored the initiation of β-catenin signaling in engineered hydrogels lacking the HAVDI motif. Without the HAVDI peptide, we reasoned that only hydrogels that induce neurosphere formation (and hence a large amount of cell-cell contacts) would be able to initiate β-catenin signaling. Consistent with this idea, in RGD-only gels, NPCs exhibited significantly increased β-catenin signaling in both Dynamic Fast and Dynamic Slow gels compared to Static gels (Fig. 3d, e). Thus, the single cells found in Static RGD gels were unable to initiate β-catenin signaling.

In contrast, the single cells grown in Dynamic Fast RGD-HAVDI hydrogels were able to initiate expression of the β-catenin-reporter *Axin2* gene (Fig. 3f). Interestingly, expression levels of *Axin2* were similar across all viscoelastic gel formulations, including Dynamic Slow and Dynamic Fast gels with RGD-RDG ligands, RGD-HAVDI ligands, and HAVDI-RDG ligands. These data suggest that similar levels of β-catenin signaling are possible for cultures that form neurospheres and cultures that remain as singularized cells when the HAVDI ligand is present in a fast stress-relaxing hydrogel. Interestingly, NPCs encapsulated within Static RGD-HAVDI hydrogels exhibited decreased expression of *Axin2* (Supplementary Fig. 8a), suggesting that a viscoelastic environment might be required for the HAVDI motifs to stimulate N-cadherin cell-surface receptors. Immunostaining and immunoblotting also revealed

https://doi.org/10.1038/s41467-025-60540-8

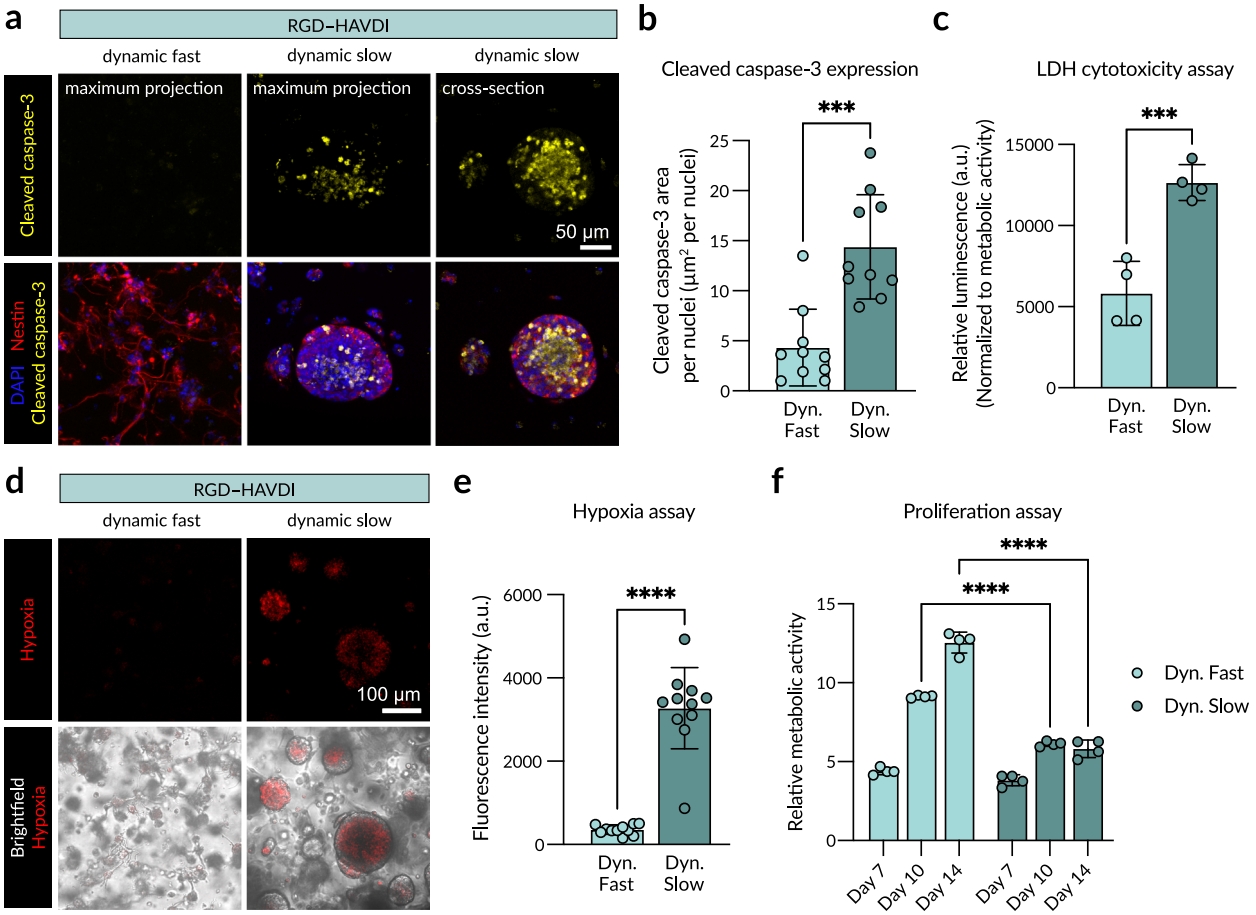

Fig. 4 | NPCs in neurospheres exhibit limited expansion due to hypoxia and cell death, whereas distributed NPC cultures maintain viability and proliferation over long-term culture. a Representative maximum projection (left and center) and single z-plane cross-section (right) fluorescence images of NPCs encapsulated within Dynamic Fast and Dynamic Slow RGD-HAVDI HELP gels after 14 days of culture labeled with Nestin (red) and cleaved caspase-3 (yellow), with nuclei counterstained (blue). **b** Quantification of cleaved caspase-3 area, normalized by cell number, after 14 days in culture. Each data point represents the average cleaved caspase-3 area per nucleus from one confocal z-stack containing several cells or neurospheres ($N = 3$ replicate hydrogels, data are means ± standard deviation). $^{***}p = 0.0001$. **c** LDH cytotoxicity assay, normalized to metabolic activity, after 14 days in culture ($N = 4$ replicate hydrogels, data are means ± standard deviation). $^{***}p = 0.0009$. **d** Representative brightfield and fluorescence images of NPCs encapsulated within Dynamic Fast and Dynamic Slow RGD-HAVDI HELP gels after 14 days of culture labeled with a fluorogenic hypoxia probe (red). **e** Quantification of fluorescence intensity of cultures stained with hypoxia probe. Each data point represents the fluorescence intensity from one confocal z-stack containing several cells or neurospheres ($N = 3$ replicate hydrogels, data are means ± standard deviation). $^{****}p < 0.0001$. **f** Quantification of the relative metabolic activity of encapsulated NPCs at days 7, 10, and 14, relative to the activity 1 hour post-encapsulation ($N = 4$ replicate hydrogels, data are means ± standard deviation). $^{****}p < 0.0001$. Statistical analyses performed as two-tailed unpaired t test (**b**, **c**, **e**) and two-way ANOVA with Šídák's multiple comparisons test (**f**). Source data are provided as a Source Data file.

similar levels of active (non-phospho S45) β-catenin (Fig. 3g, Supplementary Fig. 8b, c) and Axin2 (Supplementary Fig. 8d) across all viscoelastic hydrogel conditions, both in gel conditions that promote neurosphere growth and gel conditions that enable the growth of distributed cells. Notably, singularized NPCs within Dynamic Fast RGD-HAVDI hydrogels exhibited active β-catenin expression at statistically similar levels to those that formed neurospheres (Fig. 3g, h). Therefore, matrix presentation of HAVDI within Dynamic Fast RGD-HAVDI hydrogels appears to artificially induce downstream β-catenin signaling within a distributed 3D culture of NPCs that has limited cell-cell contact.

Distributed 3D NPC cultures support long-term NPC expansion

A key requirement for NPC expansion is the ability to maintain viable, self-renewing NPCs over long-term culture. One of the limitations of neurosphere culture is the limited diffusion of oxygen and nutrients through a large, cell-dense structure that often leads to the development of necrotic cores[13,14]. While all Dynamic HELP conditions were able to maintain NPC stemness (either as neurospheres or distributed cultures), we hypothesized that only the Dynamic Fast RGD-HAVDI hydrogels would support long-term NPC expansion due to the ability to maintain NPC stemness without developing necrosis. To evaluate this hypothesis, NPCs were cultured in maintenance medium for 14 days within either Dynamic Slow RGD-HAVDI gels, where NPCs robustly formed neurospheres, or Dynamic Fast RGD-HAVDI gels, where NPCs remained distributed as mostly single cells throughout the hydrogel. All hydrogels remained stable for up to 14 days in culture, with limited erosion observed for both hydrogel conditions (Supplementary Fig. 9). Importantly, NPCs within both Dynamic Fast and Dynamic Slow gels maintained expression of Nestin after 14 days in culture (Fig. 4a). As expected, NPCs that were cultured as neurospheres developed necrotic cores with apoptotic cells as evidenced by immunostaining for cleaved caspase-3 (Fig. 4a, b). In contrast, NPCs within the Dynamic Fast gels with distributed NPCs exhibited low expression of cleaved caspase-3. A lactate dehydrogenase (LDH) cytotoxicity assay also indicated significantly higher levels of cytotoxicity within Dynamic Slow cultures with large neurospheres compared to Dynamic Fast cultures with distributed NPCs (Fig. 4c).

We hypothesized that hypoxia due to limited oxygen diffusion to the neurosphere core may be the cause of the observed cell death. A fluorogenic hypoxia assay confirmed that NPCs within the Dynamic Slow gels were experiencing hypoxic conditions at significantly higher levels compared to NPCs within Dynamic Fast gels (Fig. 4d, e), supporting the notion that distributed 3D NPC cultures better support viable, self-renewing NPCs over long-term culture. Of note, NPCs within the Dynamic Slow gels did not experience apoptotic or hypoxic conditions at early time points (Supplementary Fig. 10), suggesting that long-term neurosphere culture, rather than material chemistry, limits oxygen diffusion. To directly assess the capacity for expansion within RGD-HAVDI HELP gels, a fluorescence-based assay was used to detect metabolically active cells within each culture over time (Fig. 4f). After 7 days, the relative metabolic activity between Dynamic Fast and Dynamic Slow gels remained similar. However, as the neurospheres within the Dynamic Slow gels continued to grow larger, the overall metabolic activity stopped increasing and plateaued at day 10. In contrast, NPCs within the Dynamic Fast gels were able to continue expanding through day 14, as evidenced by the monotonic increase in overall metabolic activity. These data suggest that at day 10, the oxygen demands outpace the diffusion rate within neurosphere cultures, as the neurospheres become hypoxic and exhibit limited expansion. When NPCs are distributed throughout the hydrogel, the diffusion rate is no longer limiting, allowing for continued NPC proliferation. Together, these data reveal that Dynamic Fast RGD-HAVDI gels that enable distributed NPC cultures throughout the hydrogel are critical for maintaining viability for long-term NPC expansion.

To further confirm that Dynamic Fast RGD-HAVDI gels are able to support long-term NPC expansion, we evaluated the ability of NPCs to maintain their viability and stem-like phenotype after being passaged from the hydrogels. NPCs were seeded either on 2D tissue culture plastic (TCP) or in 3D Dynamic Fast RGD-HAVDI gels and cultured in maintenance medium for 7 days. On day 7, NPCs on 2D TCP were passaged, and the 3D HELP gels were degraded via a brief hyaluronidase and elastase treatment to retrieve the encapsulated NPCs. Both conditions were then reseeded onto TCP for 72 hours before assessing viability, morphology, and expression of stemness markers (Supplementary Fig. 11a). The 3D passaging process resulted in high viability (> 95%), similar to when NPCs are routinely passaged in 2D (Supplementary Fig. 11b, c). In both cases, Nestin+/Sox+ NPCs were observed by immunostaining 72 hours after passage (Supplementary Fig. 11d), indicating that NPCs were able to maintain their stemness after being retrieved from 3D gels. While Nestin+/Sox+ NPCs were also observed in the 2D TCP condition, transcriptomic analyses revealed that NPCs passaged from 2D TCP altered their gene expression of several NPC stemness (*Nestin*, *Sox2*) and pro-neuronal differentiation (*NeuroD1*, *DCX*) markers (Supplementary Fig. 11e). In particular, *Nestin* levels exhibited a 2-fold decrease whereas *Sox2* levels were 24 times higher compared to NPCs prior to seeding on TCP. TCP-passaged NPCs also significantly upregulated their expression of early neuronal markers *NeuroD1* (5-fold) and *DCX* (46-fold), suggesting that the NPCs may be beginning to undergo spontaneous differentiation in 2D. In contrast, NPCs cultured and passaged from 3D HELP gels maintained relatively constant expression of *Nestin*, *Sox2*, and *NeuroD1* and a slight increase (6-fold) in *DCX* (Supplementary Fig. 11f). These differences in gene expression were also accompanied by morphological differences (Supplementary Fig. 11d). Distributed NPCs passaged from 3D HELP gels maintained their characteristic spindle-shaped morphology. Interestingly, NPCs passed from 2D TCP displayed an aberrant morphology, often with a single Nestin+ neurite at one end and diffuse Nestin signal at the opposing end. These results indicate that NPCs can be retrieved from Dynamic Fast RGD-HAVDI gels while maintaining their stem-like phenotype, supporting the use of these HELP gels for long-term expansion of NPCs.

Distributed 3D NPC cultures enhance neural differentiation

In addition to maintaining expression of stem cell markers and self-renewal capacity, stem cell function also includes maintaining multipotency. Thus, an additional functional output for NPC stemness maintenance includes the capacity to differentiate into multiple neural cell types, such as neurons and astrocytes. We hypothesized that distributed NPC cultures would result in more efficient neural differentiation, as NPCs in neurospheres may yield heterogeneous cell populations due to differences in paracrine signaling at the periphery compared to the core of the neurosphere. To evaluate differentiation capacity, NPCs were cultured in Dynamic Fast HELP gels with different ligand combinations (RGD-RDG, RGD-HAVDI, and HAVDI-RDG) for 7 days in maintenance medium prior to transitioning to differentiation conditions. Differentiation was assessed by immunostaining after 14 days of total culture.

To induce astrocytic differentiation, epidermal growth factor (EGF) and basic fibroblast growth factor (FGF-2) were removed from the culture medium, which was then supplemented with bone morphogenetic protein 4 (BMP-4). After 7 days of differentiation, immunostaining of S100 calcium-binding protein B (S100β) and glial fibrillary acidic protein (GFAP) was used to indicate astrocytic differentiation (Fig. 5a). To induce neuronal differentiation, EGF and FGF-2 were removed from the culture medium. Immunostaining of βIII-tubulin and microtubule-associated protein 2 (MAP2) was used to indicate neuronal differentiation (Fig. 5b). While some NPCs within all Dynamic Fast conditions were capable of undergoing both astrocytic and neuronal differentiation, closer inspection revealed differences in differentiation efficiency depending on ligand presentation. Specifically, NPCs that formed neurospheres within RGD-RDG and HAVDI-RDG hydrogels displayed more heterogeneous expression of differentiation markers compared to NPCs that remained distributed throughout the RGD-HAVDI hydrogels (Fig. 5c, d, Supplementary Fig. 12a, b). Neurospheres exhibited increased expression of differentiation markers in cells at the periphery, whereas expression was lower for cells within the neurosphere. The decreased expression at the neurosphere core could potentially be due to deteriorating cell health from limited oxygen, decreased nutrient diffusion, and/or changes in paracrine signaling and morphogen exposure (Fig. 4a). In contrast, distributed NPCs within RGD-HAVDI hydrogels exhibited more uniform expression of astrocytic and neuronal differentiation markers throughout the culture. This more uniform expression for distributed NPCs correlated with a significantly increased expression of both astrocytic (GFAP, Fig. 5e; S100β, Supplementary Fig. 12c) and neuronal (MAP2, Fig. 5f) differentiation markers on a per cell basis compared to the hydrogel conditions with neurospheres.

The morphology and expression of neuronal markers MAP2 and βIII-tubulin suggest that culturing NPCs within Dynamic Fast RGD-HAVDI gels may enhance their functional differentiation. Therefore, we next cultured NPCs in RGD-HAVDI gels for 7 days in maintenance medium, followed by 2 weeks in neuronal differentiation medium to allow for further neuronal maturation. To assess neuronal differentiation at a functional level, we first performed immunostaining for post-synaptic (PSD95) and pre-synaptic (synapsin, SYN1) markers. Neurons differentiated within Dynamic Fast RGD-HAVDI gels as distributed 3D cultures exhibited both post-synaptic and pre-synaptic proteins properly distributed along βIII-tubulin+ neuronal processes (Fig. 6a). In contrast, when neurons were differentiated as neurospheres in Dynamic Slow RGD-HAVDI gels, there was limited expression of synaptic markers, even in the βIII-tubulin+ regions of the neurosphere (Fig. 6b). Overall, the expression of both PSD95 and SYN1 were significantly higher in the Dynamic Fast RGD-HAVDI gels compared to the Dynamic Slow RGD-HAVDI gels (Supplementary Fig. 12d, e).

https://doi.org/10.1038/s41467-025-60540-8

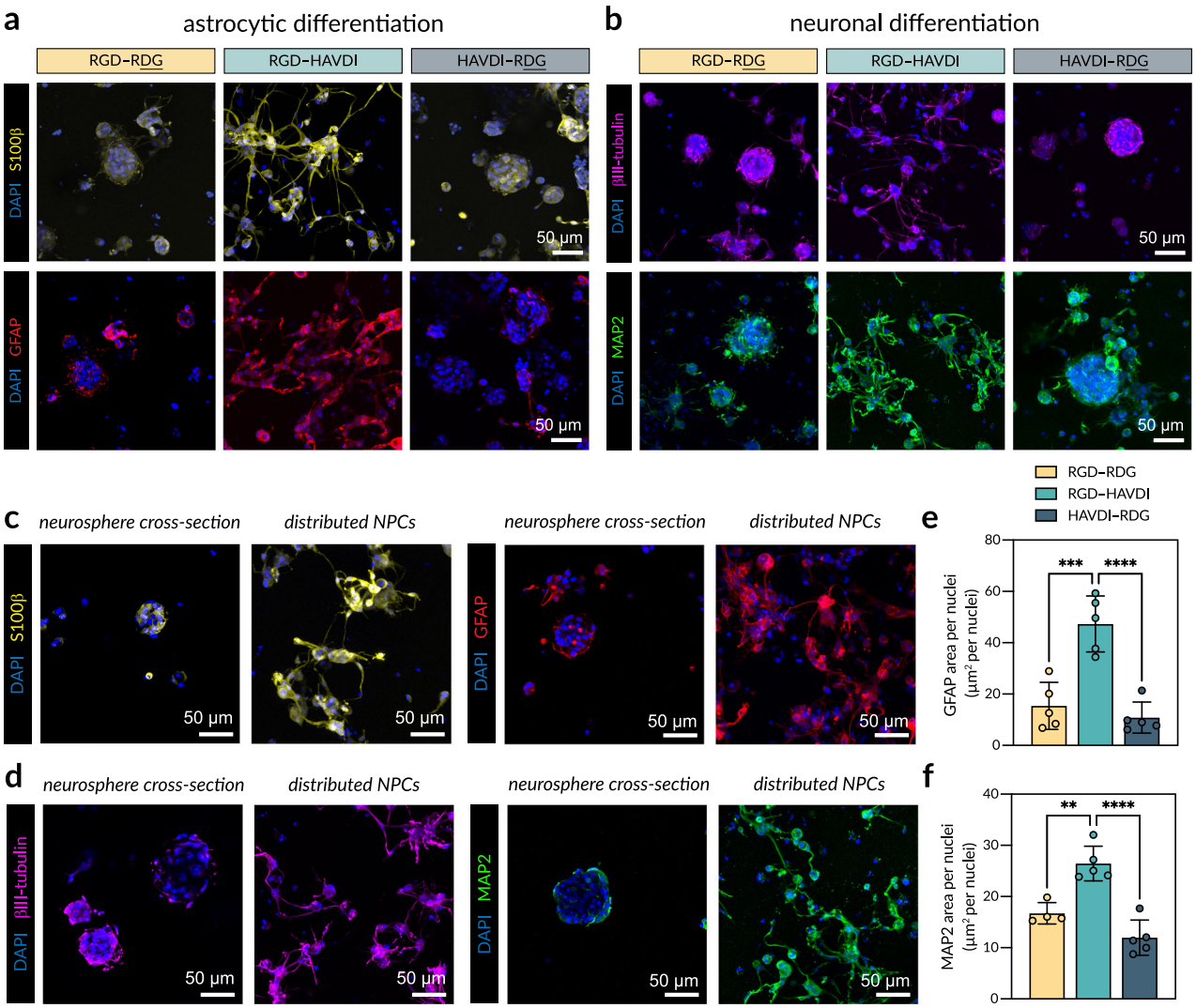

Fig. 5 | Neurosphere formation leads to heterogeneous, limited neural differentiation, whereas distributed 3D NPC cultures enhance neural differentiation. Representative maximum projection fluorescence images of NPCs within Dynamic Fast HELP gels after 7 days of (**a**) astrocytic differentiation or (**b**) neuronal differentiation. **a** Immunolabeling for the astrocytic markers S100β (yellow) and GFAP (red), with nuclei counterstained (blue). **b** Immunolabeling for the neuronal markers βIII-tubulin (magenta) and MAP2 (green), with nuclei counterstained (blue). Single z-plane fluorescence images of neurospheres compared to maximum projection fluorescence images of distributed NPCs within Dynamic Fast HELP gels after 7 days of (**c**) astrocytic differentiation or (**d**) neuronal differentiation. **c** Immunolabeling for the astrocytic markers S100β (yellow) and GFAP (red), with nuclei counterstained (blue). **d** Immunolabeling for the neuronal markers βIII-tubulin (magenta) and MAP2 (green), with nuclei counterstained (blue). Quantification of (**e**) GFAP or (**f**) MAP2 expression area, normalized by cell number ($N = 4–5$ replicate hydrogels, data are means ± standard deviation). GFAP: RGD-RDG vs. RGD-HAVDI ***$p = 0.0003$, RGD-HAVDI vs. HAVDI-RDG ****$p < 0.0001$; MAP2: RGD-RDG vs. RGD-HAVDI **$p = 0.0018$, RGD-HAVDI vs. HAVDI-RDG ****$p < 0.0001$. Statistical analyses performed as one-way ANOVA with Tukey's multiple comparisons test (**e**, **f**). Source data are provided as a Source Data file.

As additional evidence of neuronal maturation, we evaluated the ability of neurons differentiated within Dynamic Fast RGD-HAVDI gels to conduct signals via ion currents. Differentiated neurons are neurotransmitter-responsive and exhibit experimentally measurable changes in intracellular calcium levels[65–67]. Therefore, we evaluated changes in intracellular calcium concentration by time-lapse microscopy in response to stimulation by the neurotransmitter γ-aminobutyric acid (GABA). Consistent with previous studies encapsulating NPCs within 3D collagen gels or 3D ELP gels[27,68], different types of calcium transients were observed upon neurotransmitter stimulation within Dynamic Fast RGD-HAVDI gels. These included: (1) short duration increases in intracellular calcium concentration that then returned to baseline and (2) a series of consecutive spikes in intracellular calcium concentration (Fig. 6c, Supplementary Movie 1). In comparison, minimal calcium fluxes were observed in Dynamic Slow RGD-HAVDI gels (Supplementary Movie 2). Together, these results indicate that remodelable hydrogels presenting both ECM-derived integrin ligands and N-cadherin-like peptides promoted 3D distributed cultures of NPCs, which in turn permit their neuronal differentiation and maturation.

Discussion

These studies have identified the synergistic effects of matrix stress relaxation and matrix-induced N-cadherin signaling on regulating NPC morphology, stemness maintenance, and differentiation potential. Importantly, the proclivity for NPCs to form hypoxic, heterogeneous neurospheres in vitro was mitigated when both fibronectin-derived RGD ligands and N-cadherin-derived HAVDI ligands were incorporated within our fast-relaxing, viscoelastic hydrogel. Within these Dynamic Fast RGD-HAVDI hydrogels, NPCs proliferated and expanded as

https://doi.org/10.1038/s41467-025-60540-8

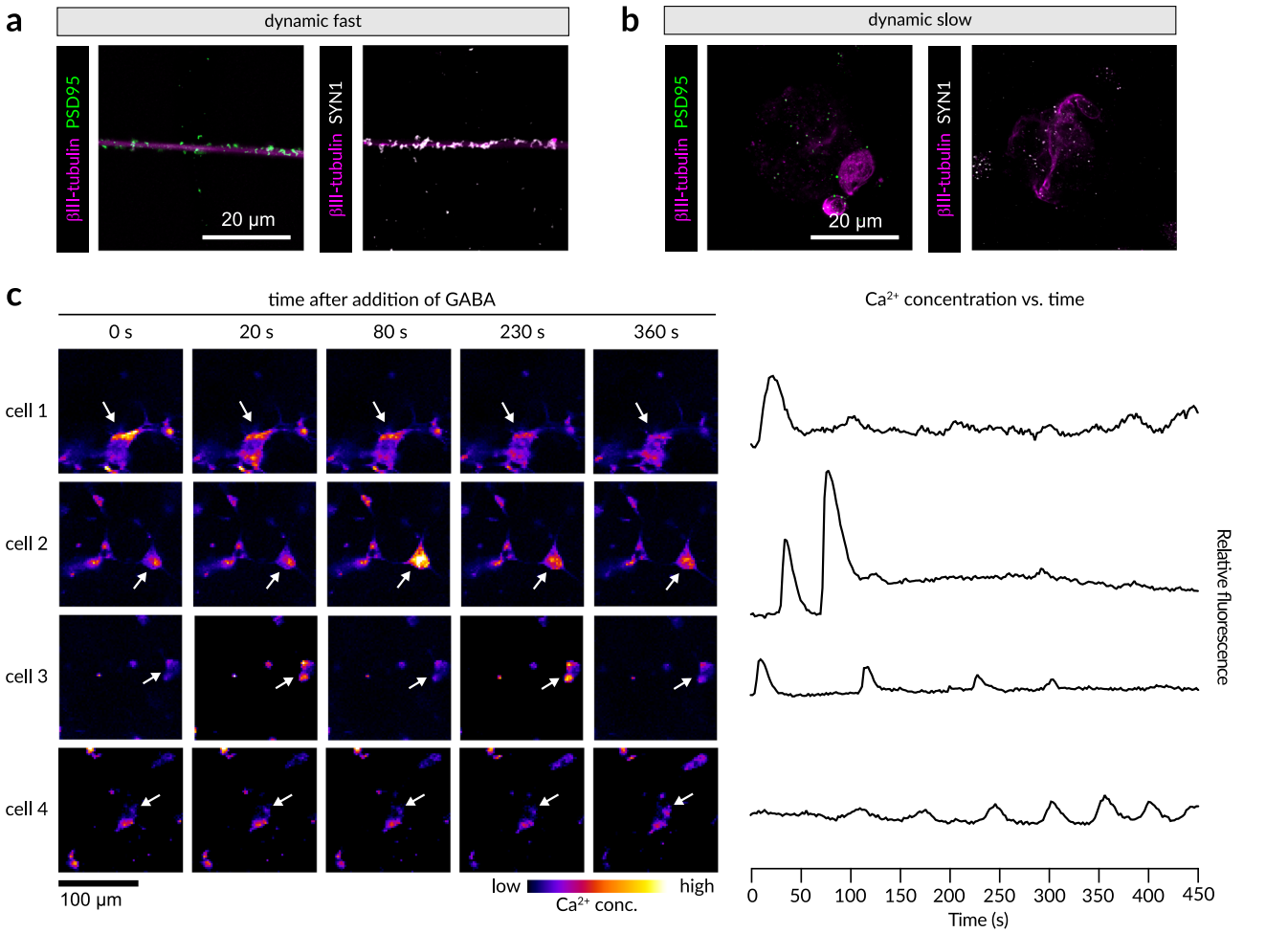

Fig. 6 | NPCs differentiated from distributed 3D NPC cultures mature into functional neurons. Representative maximum projection fluorescence images of NPC-derived neurons within Dynamic Fast (**a**) and Dynamic Slow (**b**) HELP gels after 14 days of differentiation labeled with the synaptic markers PSD95 (green) and SYN1 (white). **c** Time-lapse microscopy of four representative NPC-derived neurons within Dynamic Fast HELP gels after 14 days of differentiation incubated with the calcium-sensitive Fluo-4AM dye and treated with γ-aminobutyric acid (GABA) (left). Quantified relative fluorescence of Fluo-4AM for cells 1-4 over time (right). Source data are provided as a Source Data file.

distributed 3D cultures spread throughout the matrix. Although there was limited cell–cell contact within these distributed cultures compared to neurosphere cultures, the dispersed NPCs still maintained stemness through engagement with HAVDI ligands, which elicited N-cadherin engagement and downstream β-catenin signaling. By preventing the diffusion limitations inherent in cell-dense neurosphere cultures, distributed NPC cultures in Dynamic Fast RGD-HAVDI hydrogels exhibited long-term viability and increased expansion. Furthermore, distributed 3D NPC cultures could be expanded and differentiated within a single hydrogel platform to acquire both glial and neuronal cell fates, achieving functional neurotransmitter-responsive neurons.

In addition to serving as a stem cell niche for NPC expansion and differentiation, the culture of NPCs within 3D protein-engineered hydrogels also presents a tunable, well-defined platform for studying the combined effects of both cell-derived and matrix-derived adhesion signaling. NPCs interact with their surroundings through both cell–cell and cell–ECM interactions. However, conventional biomaterials primarily focus solely on recapitulating the properties of the ECM. This hydrogel system integrates cadherin-based motifs (cell–cell) with integrin-based motifs (cell–ECM), revealing that both are required for maintaining NPC stemness in distributed 3D cultures. Within these Dynamic Fast RGD-HAVDI HELP gels, HAVDI ligands activate downstream β-catenin signaling to a similar extent as true N-cadherin-based cell–cell contacts, thereby enabling stemness maintenance of NPCs. Interestingly, RGD is also required to prevent neurosphere formation and maintain a distributed 3D culture. While RGD alone has not been explicitly implicated in maintaining NPC stemness, RGD has been shown to promote NPC adhesion, proliferation, and neurite outgrowth[36,69,70]. A recent study showed that cells significantly slowed their migration when cultured on a cadherin-functionalized surface compared to when cultured atop matrix proteins[71]; this suggests that cell migration may be altered in the HAVDI-RDG gels that prevents NPC dispersal throughout the matrix. This idea is consistent with reports from others that HAVDI and RGD ligands may be synergistic when presented together in synthetic matrices[46,48,61]. Thus, future work could explore the synergistic effects of RGD and HAVDI ligands on NPC migration in 3D.

Another interesting finding is that Dynamic Fast RGD-HAVDI hydrogels, but not Static RGD-HAVDI hydrogels, are required for β-catenin signaling through the HAVDI peptide. One potential explanation for these results is that the faster stress-relaxing hydrogels enable dynamic ligand rearrangement. Analogous to integrin clustering in cell–matrix adhesions, cadherins also cluster during the formation of adherens junctions on the cell membrane[72,73]. Previous work with integrin receptors has demonstrated that ligand mobility and clustering play important roles in driving the acquisition of different cell fates[30,74,75]. Therefore, we postulate that within our HELP system, cells

within the Dynamic Fast HELP hydrogels may be actively rearranging and clustering the RGD and HAVDI ligands, and that ligand mobility would be much more limited in the Static HELP system. While ligand mobility and stress relaxation rate are linked within the hydrogel system used here, future work could explore the development of new biomaterials to disentangle the roles of ligand mobility and stress relaxation.

Here, the HELP platform enables independent tuning of cell-instructive ligands and matrix mechanics, enabling systematic studies of adhesion signaling in different viscoelastic contexts. One limitation of this system, however, is the range of matrix stress relaxation rates achievable. While native brain tissue has a stress relaxation half-life on the order of ~10^2 s, the stress relaxation half-life of the Dynamic Fast condition is ~10^4 s. Future studies could investigate this signaling crosstalk at faster, more physiological matrix stress relaxation rates, such as those reported for native brain tissue. Additionally, while this study makes use of two different cell-instructive ligands, the modularity of the HELP hydrogel system could enable the further exploration of the combinatorial effects of additional cell-instructive peptides for guiding NPC differentiation or alternative cadherin-derived motifs that may engage with other cell types.

Overall, this work presents a hydrogel system wherein cell-instructive ligands and matrix stress relaxation rate can be independently tuned. Encapsulation of adult NPCs in a viscoelastic hydrogel presenting both integrin-binding and cadherin-binding motifs enabled their expansion as a distributed 3D culture. We anticipate that these results will be influential in designing instructive biomaterials that take into account both biophysical and biochemical matrix properties for clinically relevant stem cell expansion.

Methods

ELP expression and characterization

ELPs containing the RGD and RDG motifs were recombinantly expressed and purified, as previously described[76]. BL21(DE3)pLysS *Escherichia coli* (Invitrogen) were transformed with a pET15b plasmid encoding the ELP sequence. Single transformed colonies were selected and cultured in autoclaved growth medium (Terrific Broth (Thermo Fisher) supplemented with 0.4% glycerol (Thermo Fisher) and 100 μg/mL ampicillin) at 37 °C overnight. The next day, 20 mL of overnight culture were transferred to each of twelve baffled flasks containing 1 L autoclaved growth medium. Cells were cultured at 37 °C under constant agitation until an optical density (λ = 600 nm) of 0.6 was reached. The temperature was then lowered to 32 °C until an optical density (λ = 600 nm) of 0.8, at which point ELP expression was induced by 1 mM isopropyl β-d-1-thiogalactopyranoside (Thermo Fisher). After 7 hours, cultures were harvested by centrifugation, resuspended in TEN buffer (10 mM Tris Base, 100 mM NaCl, and 1 mM EDTA, pH 8.0), and frozen at −80 °C. Cells were lysed through 3 freeze-thaw cycles and incubated with 10 μM deoxyribonuclease I (Sigma Aldrich) and 1 mM phenylmethanesulfonyl fluoride (PMSF; Thermo Fisher).

ELPs were purified with 3 rounds of thermal cycling. For each round, the pH of the sample was adjusted to 9.0 prior to the cold spin (15,000 x *g*, 4 °C, 1 hour). Subsequently, 1 M NaCl was added to the supernatant and agitated at 37 °C for 3 hours prior to the hot spin (15,000 x g, 37 °C, 1 hour). The resulting pellet was solubilized in ultrapure water and allowed to dissolve overnight at 4 °C. After 3 rounds, one last cold spin was performed, and the resulting supernatant was dialyzed against ultrapure water in 10 kDa molecular weight cutoff (MWCO) dialysis tubing for 3 days. Samples were subsequently lyophilized and stored at −20 °C.

The expression and purification of ELP containing the HAVDI motif was similar to the above protocol with the following differences: plasmids were transformed into BL21 Star™ (DE3)pLysS *Escherichia coli*, ELP was expressed for 24 hours at 25 °C, and 0.5 M ammonium sulfate was used for purification.

Synthesis of hydrazine-functionalized ELP

ELP was modified with hydrazine as previously described[51]. Lyophilized ELP was dissolved at 7.3% (w/v) in anhydrous dimethyl sulfoxide (DMSO; Sigma Aldrich) at room temperature (RT). After dissolution, an equal volume of anhydrous *N,N*-dimethylformamide (DMF; Sigma Aldrich) was added. In a separate flask, tri-Boc-hydrazinoacetic acid (2.1 eq. per ELP amine; Sigma Aldrich) and hexafluorophosphate azabenzotriazole tetramethyl uronium (HATU; 2 eq. per ELP amine; Sigma Aldrich) were dissolved in the same volume of anhydrous DMF used to dissolve the ELP. After dissolution, 4-methylmorpholine (5 eq. per ELP amine; Sigma Aldrich) was added and allowed to react for 10 min at RT. The tri-Boc-hydrazinoacetic acid solution was then transferred dropwise into the ELP solution and allowed to react overnight at RT under constant agitation. The next day, the reaction was precipitated in ice-cold diethyl ether (Thermo Fisher), pelleted by centrifugation, and dried under nitrogen gas to yield Boc-protected ELP. The Boc protecting groups were removed by resuspending the dried pellet in 1:1 dichloromethane (DCM; Sigma Aldrich):trifluoroacetic acid (TFA; Sigma Aldrich) supplemented with 5% (v/v) triisopropylsilane (Sigma Aldrich). The reaction was stirred for 4 hours at RT in a vented flask, precipitated in ice-cold diethyl ether, pelleted by centrifugation, and dried under nitrogen gas to yield hydrazine-functionalized ELP. The dried pellet was solubilized in ultrapure water and dialyzed against ultrapure water in 10 kDa MWCO dialysis tubing for 3 days. Samples were subsequently sterile filtered, lyophilized, and stored at −20 °C.

Synthesis of norbornene-functionalized ELP

ELP was modified with norbornene as previously described[25]. Lyophilized ELP was dissolved at 7.5% (w/v) in anhydrous DMSO at RT. After dissolution, an equal volume of anhydrous DMF was added. In a separate flask, t-Boc-*N*-amido-PEG12-acid (2 eq. per ELP amine; BroadPharm) and HATU (2.2 eq. per ELP amine) were dissolved in the same volume of anhydrous DMF used to dissolve the ELP. After dissolution, 4-methylmorpholine (5 eq. per ELP amine) was added and allowed to react for 10 min at RT. The t-Boc-*N*-amido-PEG12-acid solution was then transferred slowly into the ELP solution over the course of 10 min and allowed to react overnight at RT under constant agitation. The next day, the reaction was precipitated in ice-cold diethyl ether, pelleted by centrifugation, and dried under nitrogen gas. The Boc protecting groups were removed following the same protocol as the hydrazine-functionalized ELP to yield a PEG-functionalized ELP. The dried pellet was solubilized in ultrapure water, dialyzed against ultrapure water in 10 kDa MWCO dialysis tubing for 3 days, and lyophilized.

For norbornene conjugation, the lyophilized PEG-functionalized ELP was dissolved at 7.5% (w/v) in anhydrous DMSO at RT. After dissolution, an equal volume of anhydrous DMF was added. In a separate flask, exo-5-norbornene carboxylic acid (2 eq. per ELP amine; Sigma Aldrich) and HATU (2.2 eq. per ELP amine) were dissolved in the same volume of anhydrous DMF used to dissolve the ELP. After dissolution, 4-methylmorpholine (5 eq. per ELP amine) was added and allowed to react for 10 min at RT. The exo-5-norbornene carboxylic acid solution was then transferred slowly into the ELP solution over the course of 10 min and allowed to react overnight at RT under constant agitation. The next day, the reaction was precipitated in ice-cold diethyl ether, pelleted by centrifugation, and dried under nitrogen gas to yield norbornene-functionalized ELP. The dried pellet was solubilized in ultrapure water and dialyzed against ultrapure water in 10 kDa MWCO dialysis tubing for 3 days. Samples were subsequently sterile filtered, lyophilized, and stored at −20 °C.

Synthesis of benzaldehyde- and aldehyde-functionalized HA

HA was modified with benzaldehyde and aldehyde as previously described[25,77]. First, 100 kDa sodium hyaluronate (HA; LifeCore) was functionalized via EDC chemistry to form an HA-alkyne intermediate

polymer. Briefly, HA was dissolved at 1% (w/v) in MES buffer (0.2 M MES hydrate (Sigma Aldrich), 0.15 M NaCl, pH 4.5) at RT. After dissolution, propargylamine (0.8 eq. per HA dimer unit; Sigma Aldrich) was added, and the pH was immediately adjusted to 6.0. *N*-hydroxysuccinimide (NHS; 0.8 eq. per HA dimer unit; Thermo Fisher) and 1-ethyl-3-(3-dimethylaminopropyl)carbodiimide hydrochloride (EDC; 0.8 eq. per HA dimer unit; Thermo Fisher) were then added sequentially, and the reaction was allowed to proceed overnight at RT under constant agitation. The reaction was then dialyzed against ultrapure water in 10 kDa MWCO dialysis tubing for 3 days, sterile filtered, lyophilized, and stored at −20 °C.

The conjugation of benzaldehyde and aldehyde functional groups occurred through a subsequent copper-catalyzed azide-alkyne click chemistry reaction of either a small-molecule azidobenzaldehyde (synthesis previously described[77]) or Ald-CH2-PEG3-azide (BroadPharm) to achieve benzaldehyde- or aldehyde-functionalized HA, respectively. Briefly, lyophilized HA-alkyne was dissolved at 1% (w/v) in 10x isotonic phosphate-buffered saline (PBS; 81 mM sodium phosphate dibasic, 19 mM sodium phosphate monobasic, 60 mM sodium chloride, pH 7.4) supplemented with 1 mg/mL β-cyclodextrin (Sigma Aldrich) at RT. After dissolution, the reaction mixture was degassed under nitrogen for 30 min. Degassed solutions of sodium ascorbate (Sigma Aldrich) and copper (II) sulfate pentahydrate (Sigma Aldrich) were then added sequentially to final concentrations of 4.52 and 0.24 mM, respectively. For benzaldehyde-functionalized HA, synthesized azidobenzaldehyde (2 eq. per alkyne group) was dissolved in anhydrous DMSO and added to the reaction vessel. For aldehyde-functionalized HA, Ald-CH2-PEG3-azide (2 eq. per alkyne group) was directly added to the reaction vessel. The solution was degassed for an additional 10 min, and then the reaction was allowed to proceed for 24 hours at RT under constant agitation in the dark. After 24 hours, an equal volume of 50 mM EDTA (pH 7.0) was added to chelate the copper for 1 hour at RT. The reaction was then dialyzed against ultrapure water in 10 kDa MWCO dialysis tubing for 3 days, sterile filtered, lyophilized, and stored at −20 °C.

Synthesis of tetrazine-functionalized HA

HA was modified with tetrazine as previously described[25]. 100 kDa HA dissolved at 1% (w/v) in 0.1 M MES hydrate (pH 7.0) at RT. After dissolution, 1-hydrozybenzotriazole hydrate (2 eq. per HA dimer unit; Sigma Aldrich) was added and allowed to dissolve for 15 min. In a separate flask, tetrazine amine (2 eq. per HA dimer unit; Conju-Probe) was dissolved in a 5:1 mixture of acetonitrile (MeCN; Sigma Aldrich) and deionized water. After dissolution, EDC (2 eq. per HA dimer unit) was added. The tetrazine amine solution was then transferred slowly into the HA solution over the course of 30 min and allowed to react overnight at RT under constant agitation. The reaction was dialyzed against a 10% MeCN solution in 10 kDa MWCO dialysis tubing for 2 days, followed by ultrapure water for 3 days. Samples were subsequently sterile filtered, lyophilized, and stored at −20 °C.

HELP gel formation

Lyophilized ELP and HA were separately dissolved in 10x isotonic PBS at 2% (w/v) overnight at 4 °C. Once dissolved, the solutions were kept on ice until use. For Static HELP gels, an equal volume of ELP and HA solutions was mixed together in a tube, and 10 μL of the resulting mixture was pipetted into each custom-made silicone mold (4 mm diameter, 0.8 mm height, plasma bonded to a 12-mm circular #2 glass coverslip, Electron Microscopy Sciences). The gels were immediately incubated on ice for 5 min, RT for 15 min, then 37 °C for 10 min. For Dynamic HELP gels, 5 μL of HA was first pipetted into each custom-made silicone mold and placed on ice. An equal volume of ELP was then added to each mold and immediately mixed with the same pipette tip in circular motions. The gels were immediately incubated at RT for 15 min followed by 37 °C for 10 min.

Hydrogel rheological characterization

Shear rheology was performed using a stress-controlled ARG2 rheometer (TA instruments) with a cone-on-plate geometry (20 mm, 1° cone angle). Hydrogel samples of 48 μL were deposited on the rheometer stage, and heavy mineral oil was used to ensure hydration over the course of all measurements. Samples were allowed to crosslink under 1% oscillatory strain and 1 rad/s angular frequency following the specified gelation protocol for each gel (see *HELP gel formation*). Gels were incubated for an additional 15 min at 37 °C complete crosslinking. To evaluate the elastic properties of our hydrogels, a frequency sweep was performed from 0.1 to 100 rad/s under 1% oscillatory strain at 37 °C. The storage and loss moduli were reported from the values at 1 rad/s from these measurements. Following the frequency sweep, the samples were incubated at 37 °C for 5 min under 1% oscillatory strain and 1 rad/s to allow the rheometer geometry to equilibrate. To evaluate the stress relaxation behavior of our hydrogels, the samples were placed under 10% strain and the stress was measured over a period of 24 hours. The time at which the stress drops to half its initial value was reported as the $\tau_{1/2}$. Data was collected with the TRIOS software (TA instruments).

Murine brain rheology

Fresh brain tissue was acquired from Sprague-Dawley rats (female, 24 weeks of age, RNU$^{-/-}$ athymic, Charles River Laboratories). Mechanical measurements were collected between 1 to 2 hours following resection. Each tissue was trimmed to 8-mm-diameter and 2- to 4-mm-thick sections and allowed to equilibrate to RT in PBS. Mechanical characterization was performed using a stress-controlled ARG2 rheometer with a parallel plate geometry (8 mm). To prevent slippage, a thin section of sandpaper was adhered to both the rheometer stage and the geometry head. To perform the measurements, the geometry head was lowered onto the tissue until the normal force reached a value of 0.1 to 0.2 N. Storage moduli and stress relaxation data were then obtained as described above.

NPC culture

Adult hippocampal murine NPCs micro-dissected from the dentate gyrus were kindly provided by Prof. Theo Palmer (Stanford Neurosurgery)[78]. NPCs were cultured in NPC maintenance medium consisting of Neurobasal-A (Thermo Fisher), B-27 supplement (2%, Thermo Fisher), and GlutaMAX (1%, Thermo Fisher), supplemented with fresh 20 ng/mL FGF-2 (PeproTech) and 20 ng/mL EGF (PeproTech) on polyornithine- and laminin-coated tissue culture plastic. Before encapsulation, cells were trypsinized, pelleted, resuspended, and counted. The cell pellet was resuspended in a 2% (w/v) ELP solution at 2x the desired final cell density (i.e., 8 ×103 cells/μL for a final cell density of 4 × 103 cells/μL). HELP gels were formed as described above, and then 1 mL of maintenance media was added to each well of a 24-well plate, which contained one 10 μL gel. The culture medium was replenished every other day. To induce astrocytic differentiation, the culture medium was replaced with Neurobasal-A, 2% B-27 supplement, and 1% GlutaMAX, supplemented with fresh 20 ng/mL BMP-4 (PeproTech). To induce neuronal differentiation, the culture medium was replaced with Neurobasal-A, 2% B-27 supplement, and 1% GlutaMAX.

Hydrogel erosion

HELP gels were formulated with 0.9% ELP-hydrazine, 0.1% Cy5-conjugated ELP-hydrazine, and 1% HA (functionalized with either aldehyde or benzaldehyde) in 4 mm molds as described above. After gelation, 1 mL of maintenance media was added to each gel. At the indicated time points (Fig. S9), 200 μL of media was collected for fluorescent measurement, and the remainder was replaced with 1 mL of fresh media. The fluorescence intensity of the Cy5-conjugated ELP-hydrazine released into the media was measured on a plate reader

using an excitation of 640 nm and emission of 670 nm. After 14 days, the remaining hydrogels were completely degraded using hyaluronidase (2000 U/mL) and elastase (250 U/mL). The fluorescence signal from the degraded hydrogels was used to normalize the data. Data was collected with the SoftMax Pro software (Molecular Devices).

Viability and proliferation assays

To assess cell viability, NPC-laden hydrogels were incubated in a solution of PBS supplemented with 2 μM calcein-AM (Invitrogen) and 4 μM ethidium homodimer-1 (Invitrogen) for 10 min at 37 °C. The gels were washed and imaged with a confocal microscope (Leica SPE, Las-X software). Metabolic activity was measured using the alamarBlue Cell Viability Reagent (Invitrogen) following the manufacturer's protocols. To measure cell proliferation, cell lysate was first isolated by transferring the gels into Eppendorf tubes and treating them with an equal volume of PBS supplemented with hyaluronidase (2000 U/mL) and elastase (250 U/mL) for 30 min at 37 °C. The samples were then resuspended in cell lysis buffer (20 mM Tris HCl, 150 mM NaCl, 0.5% Triton X-100, pH 7.4), incubated on ice for 20 min, and stored at −80 °C until use. Cell proliferation was then characterized by quantifying the dsDNA content using the Quant-iT PicoGreen dsDNA Assay Kit (Invitrogen) following the manufacturer's protocols.

Immunocytochemistry

NPC-laden hydrogels were fixed in 4% paraformaldehyde in PBS at RT for 20 min, washed three times with PBS, and stored at 4 °C until use. Samples were permeabilized with 0.25% (v/v) Triton X-100 in PBS (PBS-T) for 1 hour at RT with gentle rocking. For blocking, samples were incubated with 5% (w/v) bovine serum albumin (BSA; Roche), 5% (v/v) goat serum (Gibco), and 0.5% Triton X-100 in PBS for 3 hours at RT with gentle rocking. Primary antibodies were diluted in antibody dilution solution, which consists of 2.5% (w/v) BSA, 2.5% (v/v) goat serum, and 0.5% Triton X-100 in PBS. Primary antibodies were incubated overnight at 4 °C with gentle rocking at the following dilutions: rabbit anti-Ki67 (1:100, Abcam, ab16667), rabbit anti-Sox2 (1:400, Cell Signaling, 23064), mouse anti-Nestin (1:400, BD Biosciences, 556309), mouse anti-N-cadherin (1:400, BD Biosciences, 610920), rabbit anti-non-phospho (active) β-catenin (Ser45) (1:1000, Cell Signaling, 19807), rabbit anti-Axin2 (1:200, Invitrogen, PA5-21093), rabbit anti-cleaved caspase-3 (1:400, Cell Signaling 9661), rabbit anti-S100β (1:500, Proteintech, 15146-1-AP, chicken anti-GFAP (1:500, Aves Labs, GFAP), chicken anti-βIII-tubulin (1:500, Aves Labs, TUJ), rabbit anti-MAP2 (1:500, Sigma Aldrich, ab5622), mouse anti-PSD-95 (1:500, NeuroMab, 75-028), rabbit anti-Synapsin I (1:500, Sigma Aldrich, ab1543). The following day, samples were washed three times with PBS-T for 30 min each, and then secondary antibodies were diluted in antibody dilution solution as follows: goat anti-rabbit Alexa Fluor 488 (1:500, Invitrogen, A-11008), goat anti-mouse Alexa Fluor 594 (1:500, Invitrogen, A-11032), goat anti-chicken Alexa Fluor 647 (1:500, Invitrogen, A-21449). 4′,6-diamidino-2-phenylindole (DAPI; 1 μg/mL, Cell Signaling, 4083s) was included in the secondary antibody solution to stain nuclei. Samples were incubated overnight at 4 °C with gentle rocking. The following day, samples were washed three times with PBS-T for 20 min each and then mounted onto no. 1 coverslips with ProLong Gold AntiFade Mountant (Thermo Fisher). After curing for 24 hours, stained hydrogels were imaged with a confocal microscope (Leica SPE, Las-X software). All images were taken at a z-depth of at least 50 μm from the coverslips to avoid possible confounds imparted by the mechanical properties of the glass.

RNA isolation and qPCR

For quantitative polymerase chain reaction (qPCR), encapsulated cells were first released from the hydrogels by transferring the gels into Eppendorf tubes and treating them with an equal volume of PBS supplemented with hyaluronidase (2000 U/mL) and elastase (250 U/mL) for 30 min at 37 °C. The samples were then resuspended in TRIzol reagent (Invitrogen) and stored at −80 °C until use. The samples were thawed on ice and disrupted by probe sonication (Heilscher UP50H, 50% amplitude (25 W), 30-kHz frequency, 0.5 s cycle). mRNA was purified using a phenol-chloroform extraction with 5PRIME phase lock gels (Quantabio) and subsequent isopropyl alcohol precipitation. After two washes with 70% ethanol, samples were then dried and resuspended in nuclease-free water. mRNA (200 ng) was reverse transcribed using the High Capacity cDNA Reverse Transcription Kit (Applied Biosystems). cDNA samples were diluted 10-fold in nuclease-free water, then 6.6 μL of cDNA per gene was mixed with 0.9 μL of 5 μM forward and reverse primer pair solution and 7.5 μL of Fast SYBR Green Master Mix (Applied Biosystems). The reaction mixture was run on a StepOnePlus Real Time PCR System, collected using the StepOne software (Applied Biosystems), and analyzed using the ΔC_T method. Primer sequences can be found in Supplementary Table 1.

Western blot

For Western blotting, encapsulated cells were first released from the hydrogels as described above. Cells were pelleted by centrifugation, the supernatant containing degraded hydrogel was removed, and the cells were resuspended in RIPA lysis buffer supplemented with 1 mM PMSF and protease inhibitor tablets (Roche). The samples were incubated on ice for 20 min and stored at −80 °C until use. The samples were thawed on ice, diluted in 5x gel loading buffer (300 mM Tris at pH 6.8, 50% glycerol, 10 wt % sodium dodecyl sulfate, and 0.05 wt % bromophenol blue) containing 500 mM dithiothreitol, and boiled for 10 min prior to separation on precast 12% polyacrylamide gels (Bio-Rad). Gels were transferred onto polyvinylidene fluoride membranes (Invitrogen) via wet transfer for 70 min at 100 V. Membranes were cut to enable staining of different molecular weight proteins from the same gel and blocked in 5% milk for 1 hour at RT. They were then incubated with the following primary antibodies diluted in 5% milk overnight at 4 °C: mouse anti-Nestin (1:1000, BD Biosciences, 556309), rabbit anti-Sox2 (1:1000, Millipore Sigma, AB5603), rabbit anti-non-phospho (active) β-catenin (Ser45) (1:1000, Cell Signaling, 19807), rabbit β-actin (1:1000, Cell Signaling, 4970). The next day, membranes were washed three times for 5 min each with TBS-T: tris-buffered saline (20x stock: 3 M NaCl and 750 mM Tris hydrochloride at pH 7.2) supplemented with 0.25% (v/v) Tween-20. They were then incubated with the appropriate horseradish peroxidase-conjugated secondary antibody (Jackson ImmunoResearch) diluted in TBS-T for 1 hour at RT. Membranes were washed four times with TBS-T for 10 min each, developed using either the SuperSignal West Pico or Femto Chemiluminescent Substrate (Thermo Fisher), and imaged using a ChemiDoc MP gel imaging system (Bio-Rad). Data was collected with the Image Lab software (Bio-Rad).

Cadherin inhibition

For cadherin blocking studies, NPCs were trypsinized and incubated in maintenance medium with 0.5 mg/mL cHAV peptide (Exherin, Adooq Biosciences) at 37 °C for 30 min under constant agitation. NPCs were then pelleted by centrifugation and encapsulated within hydrogels as described above. Encapsulated cells were cultured in maintenance medium containing 0.5 mg/mL cHAV peptide for 7 days, replacing the medium every other day.

Cytotoxicity and hypoxia assays

Cytotoxicity was characterized by measuring lactate dehydrogenase (LDH) activity. Samples of culture medium were collected in LDH storage buffer (200 mM Tris-HCl (pH 7.3), 10% glycerol, 1% BSA) and stored at −80 °C until use. The LDH-Glo Cytotoxicity Assay (Promega) was performed on the samples following the manufacturer's protocols.

Hypoxia in live cells was measured using the Image-iT Red Hypoxia Reagent (Invitrogen) following the manufacturer's protocols and then imaged using a confocal microscope (Leica SPE, Las-X software).

Passaging from HELP gels

Encapsulated cells were first released from the hydrogels by transferring the gels into Eppendorf tubes and treating them with an equal volume of PBS supplemented with hyaluronidase (2000 U/mL) and elastase (250 U/mL) for 30 min at 37 °C. Cells were pelleted by centrifugation, and the supernatant containing degraded hydrogel was removed. The resultant cell pellet was then trypsinized, pelleted, resuspended, and counted before seeding on laminin-coated plates.

Calcium imaging

NPCs were incubated with Fluo-4 AM dye (1000X, Invitrogen) and PowerLoad concentrate (100X, Invitrogen) in Neurobasal-A medium without phenol red for 1 hour at 37 °C. The hydrogel samples were then washed with normal physiological medium (145 mM NaCl, 5 mM KCl, 1.8 mM $CaCl_2$, 0.8 mM $MgCl_2$, 10 mM HEPES, 10 mM glucose, pH 7.4) and maintained in normal physiological medium at room temperature for the duration of the experiment. The samples were then placed on the microscope stage, the cells were exposed to 10 μM GABA, and immediately imaged on a confocal microscope (Leica SPE, Las-X software) by exciting at 488 nm every 2 s for 10 min. To quantify changes in intracellular calcium concentration, regions of interest were drawn around the cells in FIJI, and the integrated pixel intensity was recorded at each time point.

Image analysis

Neurosphere cluster size and number were performed using CellProfiler based on DAPI staining. Shape analysis was performed by thresholding the image, removing objects with 2D projected areas less than 400 μm^2, and calculating the diameter. The number of DAPI + nuclei, Ki67+ cells, and Sox2+ cells; the intensity of Sox2 and β-catenin; as well as the cleaved caspase-3 area, GFAP area, S100β area, and MAP2 area, were quantified using CellProfiler. Nuclei and cells were immunolabeled with the relevant markers or antibodies and identified using "IdentifyPrimaryObjects" with the "Minimum Cross-Entropy" thresholding method, followed by "MeasureImageAreaOccupied" or "MeasureObjectIntensity." Quantification on a per cell basis was done by normalizing the area of expression by the nuclei count. To characterize the length of individual neuritic projections, Nestin-expressing projections were manually traced and quantified with the SNT toolbox[79].

Statistical analysis and reproducibility

The data collected for this manuscript were obtained from over 30 distinct batches of NPC thawing to initiate encapsulated NPC cultures, four expressions and modifications of ELP, and three modifications of HA. Results were consistent across all biological and material batches. The data shown in figures are independent replicates for a given experiment. Experiments in which representative images are shown were repeated a minimum of three times. No data were excluded from the analyses. The investigators were not blinded to allocation during experiments and outcome assessment. Statistical analyses for this study were performed using GraphPad Prism version 10 software. Details of specific statistical methods for each figure are included within the figure captions. For all studies, not significant (ns; $p > 0.05$), $^{*}p < 0.05$, $^{**}p < 0.01$, $^{***}p < 0.001$, and $^{****}p < 0.0001$.

Reporting summary

Further information on research design is available in the Nature Portfolio Reporting Summary linked to this article.

Data availability

All data generated in this study have been deposited in the Stanford Digital Repository, which can be accessed through the persistent URL and the DOI (https://doi.org/10.25740/wq151qj9347). Source data are provided with this paper.

References

1. Goldman, S. Stem and progenitor cell-based therapy of the human central nervous system. *Nat. Biotechnol.* **23**, 862–871 (2005).
2. Martino, G. & Pluchino, S. The therapeutic potential of neural stem cells. *Nat. Rev. Neurosci.* **7**, 395–406 (2006).
3. Tang, Y., Yu, P. & Cheng, L. Current progress in the derivation and therapeutic application of neural stem cells. *Cell Death Dis.* **8**, e3108 (2017).
4. Trounson, A. & McDonald, C. Stem cell therapies in clinical trials: progress and challenges. *Cell Stem Cell* **17**, 11–22 (2015).
5. Bouab, M., Paliouras, G. N., Aumont, A., Forest-Bérard, K. & Fernandes, K. J. Aging of the subventricular zone neural stem cell niche: evidence for quiescence-associated changes between early and mid-adulthood. *Neuroscience* **173**, 135–149 (2011).
6. Nishino, J., Kim, I., Chada, K. & Morrison, S. J. Hmga2 promotes neural stem cell self-renewal in young but not old mice by reducing p16Ink4a and p19Arf Expression. *Cell* **135**, 227–239 (2008).
7. Ladran, I., Tran, N., Topol, A. & Brennand, K. J. Neural stem and progenitor cells in health and disease. *Wiley Interdiscip. Rev. Syst. Biol. Med* **5**, 701–715 (2013).
8. Kurtz, A. & Oh, S. J. Age related changes of the extracellular matrix and stem cell maintenance. *Prev. Med.* **54 Suppl**, S50–56, (2012).
9. Morrison, S. J. & Spradling, A. C. Stem cells and niches: mechanisms that promote stem cell maintenance throughout life. *Cell* **132**, 598–611 (2008).
10. Morawski, M., Filippov, M., Tzinia, A., Tsilibary, E. & Vargova, L. ECM in brain aging and dementia. *Prog. Brain Res.* **214**, 207–227 (2014).
11. Reynolds, B. A. & Weiss, S. Generation of neurons and astrocytes from isolated cells of the adult mammalian central nervous system. *Science* **255**, 1707–1710 (1992).
12. Ahmed, S. The culture of neural stem cells. *J. Cell Biochem.* **106**, 1–6 (2009).
13. Dmitriev, R. I., Zhdanov, A. V., Nolan, Y. M. & Papkovsky, D. B. Imaging of neurosphere oxygenation with phosphorescent probes. *Biomaterials* **34**, 9307–9317 (2013).
14. Jensen, J. B. & Parmar, M. Strengths and limitations of the neurosphere culture system. *Mol. Neurobiol.* **34**, 153–161 (2006).
15. Lei, Y. & Schaffer, D. V. A fully defined and scalable 3D culture system for human pluripotent stem cell expansion and differentiation. *Proc. Natl. Acad. Sci. USA* **110**, E5039–E5048 (2013).
16. Johnson, H. J., Chakraborty, S., Muckom, R. J., Balsara, N. P. & Schaffer, D. V. A scalable and tunable thermoreversible polymer for 3D human pluripotent stem cell biomanufacturing. *iScience* **25**, 104971 (2022).
17. Madl, C. M. et al. Maintenance of neural progenitor cell stemness in 3D hydrogels requires matrix remodelling. *Nat. Mater.* **16**, 1233–1242 (2017).
18. Roth, J. G. et al. Advancing models of neural development with biomaterials. *Nat. Rev. Neurosci.* **22**, 593–615 (2021).
19. Little, L., Healy, K. E. & Schaffer, D. Engineering biomaterials for synthetic neural stem cell microenvironments. *Chem. Rev.* **108**, 1787–1796 (2008).
20. Madl, C. M. & Heilshorn, S. C. Engineering hydrogel microenvironments to recapitulate the stem cell niche. *Annu Rev. Biomed. Eng.* **20**, 21–47 (2018).
21. Moshayedi, P. et al. Systematic optimization of an engineered hydrogel allows for selective control of human neural stem cell survival and differentiation after transplantation in the stroke brain. *Biomaterials* **105**, 145–155 (2016).

22. Lam, J., Carmichael, S. T., Lowry, W. E. & Segura, T. Hydrogel design of experiments methodology to optimize hydrogel for iPSC-NPC culture. *Adv. Health Mater.* **4**, 534–539 (2015).
23. Baek, J. et al. Egr1 is a 3D matrix-specific mediator of mechanosensitive stem cell lineage commitment. *Sci. Adv.* **8**, eabm4646 (2022).
24. Leipzig, N. D. & Shoichet, M. S. The effect of substrate stiffness on adult neural stem cell behavior. *Biomaterials* **30**, 6867–6878 (2009).
25. Roth, J. G. et al. Tunable hydrogel viscoelasticity modulates human neural maturation. *Sci. Adv.* **9**, eadh8313 (2023).
26. Qiao, E., Fulmore, C. A., Schaffer, D. V. & Kumar, S. Substrate stress relaxation regulates neural stem cell fate commitment. *Proc. Natl. Acad. Sci. USA* **121**, e2317711121 (2024).
27. Madl, C. M., LeSavage, B. L., Dewi, R. E., Lampe, K. J. & Heilshorn, S. C. Matrix remodeling enhances the differentiation capacity of neural progenitor cells in 3D hydrogels. *Adv. Sci.* **6**, 1801716 (2019).
28. Nam, S., Lee, J., Brownfield, D. G. & Chaudhuri, O. Viscoplasticity enables mechanical remodeling of matrix by cells. *Biophys. J.* **111**, 2296–2308 (2016).
29. Chaudhuri, O., Cooper-White, J., Janmey, P. A., Mooney, D. J. & Shenoy, V. B. Effects of extracellular matrix viscoelasticity on cellular behaviour. *Nature* **584**, 535–546 (2020).
30. Chaudhuri, O. et al. Hydrogels with tunable stress relaxation regulate stem cell fate and activity. *Nat. Mater.* **15**, 326–334 (2016).
31. Sinha, S., Ayushman, M., Tong, X. & Yang, F. Dynamically crosslinked Poly(ethylene-glycol) hydrogels reveal a critical role of viscoelasticity in modulating glioblastoma fates and drug responses in 3D. *Adv. Health Mater.* **12**, e2202147 (2023).
32. Zimmermann, D. R. & Dours-Zimmermann, M. T. Extracellular matrix of the central nervous system: from neglect to challenge. *Histochem. Cell Biol.* **130**, 635–653 (2008).
33. Suhar, R. A., Huang, M. S., Navarro, R. S., Aviles Rodriguez, G. & Heilshorn, S. C. A library of elastin-like proteins with tunable matrix ligands for in vitro 3D neural cell culture. *Biomacromolecules* **24**, 5926–5939 (2023).
34. MacEwan, S. R. & Chilkoti, A. Elastin-like polypeptides: biomedical applications of tunable biopolymers. *Biopolymers* **94**, 60–77 (2010).
35. Ibáñez-Fonseca, A., Flora, T., Acosta, S. & Rodríguez-Cabello, J. C. Trends in the design and use of elastin-like recombinamers as biomaterials. *Matrix Biol.* **84**, 111–126 (2019).
36. Ananthanarayanan, B., Little, L., Schaffer, D. V., Healy, K. E. & Tirrell, M. Neural stem cell adhesion and proliferation on phospholipid bilayers functionalized with RGD peptides. *Biomaterials* **31**, 8706–8715 (2010).
37. Meco, E., Zheng, W. S., Sharma, A. H. & Lampe, K. J. Guiding Oligodendrocyte precursor cell maturation with Urokinase Plasminogen activator-degradable elastin-like protein hydrogels. *Biomacromolecules* **21**, 4724–4736 (2020).
38. Galarza, S., Crosby, A. J., Pak, C. & Peyton, S. R. Control of Astrocyte quiescence and activation in a synthetic brain hydrogel. *Adv. Health Mater.* **9**, e1901419 (2020).
39. Hatta, K., Nose, A., Nagafuchi, A. & Takeichi, M. Cloning and expression of cDNA encoding a neural calcium-dependent cell adhesion molecule: its identity in the cadherin gene family. *J. Cell Biol.* **106**, 873–881 (1988).
40. Blaschuk, O. W., Sullivan, R., David, S. & Pouliot, Y. Identification of a cadherin cell adhesion recognition sequence. *Dev. Biol.* **139**, 227–229 (1990).
41. Williams, E., Williams, G., Gour, B. J., Blaschuk, O. W. & Doherty, P. A novel family of cyclic peptide antagonists suggests that N-cadherin specificity is determined by amino acids that flank the HAV motif. *J. Biol. Chem.* **275**, 4007–4012 (2000).
42. Qin, E. C. et al. Comparative effects of N-cadherin protein and peptide fragments on mesenchymal stem cell mechanotransduction and paracrine function. *Biomaterials* **239**, 119846 (2020).
43. Williams, G., Williams, E. J. & Doherty, P. Dimeric versions of two short N-cadherin binding motifs (HAVDI and INPISG) function as N-cadherin agonists. *J. Biol. Chem.* **277**, 4361–4367 (2002).
44. Bian, L., Guvendiren, M., Mauck, R. L. & Burdick, J. A. Hydrogels that mimic developmentally relevant matrix and N-cadherin interactions enhance MSC chondrogenesis. *Proc. Natl. Acad. Sci. USA* **110**, 10117–10122 (2013).
45. Zhu, M. et al. Hydrogels functionalized with N-cadherin mimetic peptide enhance osteogenesis of hMSCs by emulating the osteogenic niche. *Biomaterials* **77**, 44–52 (2016).
46. Cosgrove, B. D. et al. N-cadherin adhesive interactions modulate matrix mechanosensing and fate commitment of mesenchymal stem cells. *Nat. Mater.* **15**, 1297–1306 (2016).
47. Borelli, A. N., Schultze, C. L., Young, M. W., Kirkpatrick, B. E. & Anseth, K. S. Ligand presentation controls collective MSC response to matrix stress relaxation in hybrid PEG-HA hydrogels. *Bioact. Mater.* **44**, 152–163 (2025).
48. Baek, J., Kumar, S., Schaffer, D. V. & Im, S. G. N-Cadherin adhesive ligation regulates mechanosensitive neural stem cell lineage commitment in 3D matrices. *Biomater. Sci.* **10**, 6768–6777 (2022).
49. Kjar, A. et al. Biofunctionalized gelatin hydrogels support development and maturation of iPSC-derived cortical organoids. *Cell Rep.* **43**, (2024).
50. O'Grady, B. J. et al. Development of an N-Cadherin biofunctionalized hydrogel to support the formation of synaptically connected neural networks. *ACS Biomater. Sci. Eng.* **6**, 5811–5822 (2020).
51. Hefferon, M. E. et al. Cell microencapsulation within engineered Hyaluronan Elastin-Like Protein (HELP) hydrogels. *Curr. Protoc.* **3**, e917 (2023).
52. Elkin, B. S., Azeloglu, E. U., Costa, K. D. & Morrison, B. 3rd Mechanical heterogeneity of the rat hippocampus measured by atomic force microscope indentation. *J. Neurotrauma* **24**, 812–822 (2007).
53. Budday, S. et al. Rheological characterization of human brain tissue. *Acta Biomater.***60**, 315–329 (2017).
54. Jacques, T. S. et al. Neural precursor cell chain migration and division are regulated through different beta1 integrins. *Development* **125**, 3167–3177 (1998).
55. Leone, D. P. et al. Regulation of neural progenitor proliferation and survival by beta1 integrins. *J. Cell Sci.* **118**, 2589–2599 (2005).
56. Lampe, K. J., Antaris, A. L. & Heilshorn, S. C. Design of three-dimensional engineered protein hydrogels for tailored control of neurite growth. *Acta Biomater.* **9**, 5590–5599 (2013).
57. McKay, R. Stem cells in the central nervous system. *Science* **276**, 66–71 (1997).
58. Kriegstein, A. & Alvarez-Buylla, A. The glial nature of embryonic and adult neural stem cells. *Annu. Rev. Neurosci.* **32**, 149–184 (2009).
59. Noctor, S. C., Flint, A. C., Weissman, T. A., Dammerman, R. S. & Kriegstein, A. R. Neurons derived from radial glial cells establish radial units in neocortex. *Nature* **409**, 714–720 (2001).
60. Kadowaki, M. et al. N-cadherin mediates cortical organization in the mouse brain. *Dev. Biol.* **304**, 22–33 (2007).
61. Barcelona-Estaje, E. et al. N-cadherin crosstalk with integrin weakens the molecular clutch in response to surface viscosity. *Nat. Commun.* **15**, 8824 (2024).
62. Zhang, J. et al. Cortical neural precursors inhibit their own differentiation via N-cadherin maintenance of beta-catenin signaling. *Dev. Cell* **18**, 472–479 (2010).
63. Cai, C. et al. c-Myc regulates neural stem cell quiescence and activation by coordinating the cell cycle and mitochondrial remodeling. *Signal Transduct. Target. Ther.* **6**, 306 (2021).

64. Bizen, N. et al. A growth-promoting signaling component cyclin D1 in neural stem cells has antiastrogliogenic function to execute self-renewal. *Stem Cells* **32**, 1602–1615 (2014).
65. Lin, L., Yuan, J., Sander, B. & Golas, M. M. In vitro differentiation of human neural progenitor cells into striatal GABAergic neurons. *STEM CELLS Transl. Med.* **4**, 775–788 (2015).
66. Sharma, Y., Saha, S., Joseph, A., Krishnan, H. & Raghu, P. In vitro human stem cell derived cultures to monitor calcium signaling in neuronal development and function. *Wellcome Open Res.* **5**, 16 (2020).
67. Rosenberg, S. S. & Spitzer, N. C. Calcium signaling in neuronal development. *Cold Spring Harb. Perspect. Biol.* **3**, a004259 (2011).
68. Ma, W. et al. CNS stem and progenitor cell differentiation into functional neuronal circuits in three-dimensional collagen gels. *Exp. Neurol.* **190**, 276–288 (2004).
69. Mauri, E. et al. Evaluation of RGD functionalization in hybrid hydrogels as 3D neural stem cell culture systems. *Biomater. Sci.* **6**, 501–510 (2018).
70. Romano, N. H., Madl, C. M. & Heilshorn, S. C. Matrix RGD ligand density and L1CAM-mediated Schwann cell interactions synergistically enhance neurite outgrowth. *Acta Biomater.* **11**, 48–57 (2015).
71. Suh, K., Cho, Y. K., Breinyn, I. B. & Cohen, D. J. E-cadherin biointerfaces reprogram collective cell migration and cell cycling by forcing homeostatic conditions. *bioRxiv*, 2023.2007.2025.550505, (2023).
72. Changede, R. & Sheetz, M. Integrin and cadherin clusters: A robust way to organize adhesions for cell mechanics. *BioEssays* **39**, e201600123 (2017).
73. Thompson, C. J. et al. Cadherin clusters stabilized by a combination of specific and nonspecific cis-interactions. *Elife* **9**, e59035 (2020).
74. Álvarez, Z. et al. Artificial extracellular matrix scaffolds of mobile molecules enhance maturation of human stem cell-derived neurons. *Cell Stem Cell* **30**, 219–238.e214 (2023).
75. Roth, J. G., Huang, M. S. & Heilshorn, S. C. Mobility mediates maturation: Synthetic substrates to enhance neural differentiation. *Cell Stem Cell* **30**, 115–117 (2023).
76. LeSavage, B. L., Suhar, N. A., Madl, C. M. & Heilshorn, S. C. Production of elastin-like protein hydrogels for encapsulation and immunostaining of Cells in 3D. *JoVE* **135**, e57739 (2018).
77. LeSavage, B. L. et al. Engineered matrices reveal stiffness-mediated chemoresistance in patient-derived pancreatic cancer organoids. *Nat. Mater.* **23**, 1138–1149 (2024).
78. Babu, H., Cheung, G., Kettenmann, H., Palmer, T. D. & Kempermann, G. Enriched monolayer precursor cell cultures from micro-dissected adult mouse dentate gyrus yield functional granule cell-like neurons. *PLoS One* **2**, e388 (2007).
79. Arshadi, C., Günther, U., Eddison, M., Harrington, K. I. S. & Ferreira, T. A. SNT: a unifying toolbox for quantification of neuronal anatomy. *Nat. methods* **18**, 374–377 (2021).

Acknowledgements

The authors thank T. Palmer (Stanford Neurosurgery) for providing the murine NPCs and R. Suhar (Stanford Materials Science and Engineering) for assistance with ELP expression. M.S.H. acknowledges support from the Sarafan ChEM-H Chemistry/Biology Interface Program as an O'Leary-Thiry Fellow, a National Science Foundation (NSF) Graduate Research Fellowship (DGE-1656518), a National Institutes of Health (NIH) NRSA Pre-doctoral Fellowship (F31-NS132505) and the Gerald J. Lieberman Fellowship. B.L.L. acknowledges support from the Siebel Scholars Program and the Stanford Bio-X Bowes Graduate Fellowship. S.G. acknowledges support from the Novo Nordisk Foundation (NNF22OC0073507). J.G.R. acknowledges support from an NSF Graduate Research Fellowship (DGE-1656518) and the Stanford Smith Family Graduate Fellowship. R.S.N. acknowledges support from an NIH K99/R00 MOSAIC Postdoctoral Career Transition Award (K99-HL169844). S.C.H. acknowledges support from the NIH (R01-HL142718, R01-EB027666, R01-EB027171, R01-HL151997, R01-MH137333), NSF (DMR-2103812, CBET-2033302, DMR-2427971) and the California Institute for Regenerative Medicine (DISC2-13020). Part of this work was performed at the Stanford Nano Shared Facilities, supported by the NSF (ECCS-2026822).

Author contributions

MS.H., B.L.L. and S.C.H. conceived and initiated the project. M.S.H. designed the research, synthesized the materials, conducted the experiments and analyzed the data. B.L.L. designed and cloned the ELP containing the HAVDI motif. B.L.L., S.G., A.E.G. and J.G.R. assisted with protein expression, cell encapsulation, qRT-PCR and confocal imaging. C.H.-L. assisted with the design and execution of the cadherin inhibition experiments. E.A.M. assisted with confocal imaging. R.S.N. assisted with biomaterials synthesis and characterization. M.S.H. and S.C.H. wrote the manuscript. S.C.H. supervised the study. All authors edited and approved the manuscript.

Competing interests

S.C.H. is an inventor on a patent application (no. US2021057925) submitted by the Board of Trustees of Stanford University. All other authors declare that they have no competing interests.

Additional information

Supplementary information The online version contains supplementary material available at https://doi.org/10.1038/s41467-025-60540-8.

Correspondence and requests for materials should be addressed to Sarah C. Heilshorn.

Peer review information *Nature Communications* thanks Stephanie Seidlits, who co-reviewed with Sabrina PietrosemoliSalazarE. Pashuck, Liming Bian, Xufeng Xue, and Jennifer Young for their contribution to the peer review of this work. A peer review file is available.